Workshop: "Practical Computer Modeling for Medical Device Development"
37th IEEE Engineering in Medicine & Biology Conference, 2015
Milan, Italy

Part 6: "Including Prediction of Irreversible Thermal Alterations in Numerical Model Work"

John Pearce
Temple Foundation Professor
Department of Electrical and Computer Engineering
The University of Texas at Austin

I. Introduction:

So, given a transient temperature history, T(x, y, z, t), now what? Many investigators stop at this point and use an isotherm at some arbitrary value as an indicator of "thermal damage" or "cell death", without much critical thought. This is a weak and unsatisfying approach that often leads to unrealistic conclusions and should be avoided if it can be since it only applies for a specific heating time. The real question is: what is actually happening in the tissues? All living tissues are composed of structural and functional proteins maintained in homeostasis by complex interactions and cascades of biochemical reactions. The result of this is that the particular irreversible thermal alteration realized in a heating protocol is a kinetic process. Thermodynamics deals with state changes — from state A to state B as described by the six inter-dependent state variables, temperature, pressure, enthalpy, entropy, density and specific volume — irrespective of the rate at which the changes are taking place. The rate of change of state is described by the kinetic branch of thermodynamics; the study of process rates. The accumulation of irreversible thermal alterations is composed of multiple kinetic processes each operating in parallel and thermodynamically independently. So, it is not just the temperature, but the time of exposure as well that determines the histologic outcome. This is where the important and most useful results of numerical modeling studies are to be found. This branch of numerical modeling studies is thus heavily dependent on chemical formulations to obtain fundamental understanding. Think of it as a tour through rate-process thermodynamics if you are uncomfortable with chemistry.

In these notes, we will begin by developing models of processes that describe irreversible thermal alterations in tissue due to heating that are useful at higher temperatures and for multiple processes. High temperature damage involves relatively simple reactions that can be effectively modeled by single step irreversible Arrhenius kinetics. We then inspect intrinsic cell death processes, which depend on functional protein cascades and are considerably more complex. They consequently require substantially more complicated multiple dynamic system state-space reaction equations to describe adequately. We will see that the system reactions include reversibility and some form of delay, usually in the form of association/dissociation reaction terms. We conclude with a modified form of the Arrhenius model that incorporates a simple temperature-dependent delay to provide a more accurate prediction in the case of these more complicated intrinsic cell death processes.

II. Damage Process Fundamentals

The two most basic models of thermal damage are the "Arrhenius Kinetic Analysis" method and "Cumulative Equivalent Minutes at 43 C" (CEM_{43}), as currently typically used in tumor hyperthermia studies. The Arrhenius method is commonly used to describe burns, coagulation and surgical ablation processes and has proven effective when rapid, simple, single-step irreversible reactions are taking place — the usual case at temperatures in excess of 55 C or so. The two methods are mathematically equivalent at their origin, and can be converted, one to the other, if a suitable common end point can be established and the temperature does not exceed the CEM reference temperature by more than a few degrees. Single first-order reaction kinetics, as in these two approaches, are not effective in modeling cell death processes resulting from slow heating to moderate temperatures for long periods, particularly in the early stages, *i.e.* the slowly-developing "shoulder" region of typical cell survival curves. The single irreversible reaction kinetics methods are "constant rate" models, which cell survival curves typically exhibit in constant temperature experiments at longer times, but will over-predict cell death in the early stages of the shoulder region. The notes conclude with a brief overview of the complex sequences of reactions that characterize the four currently known intrinsic cell death processes: apoptosis,[1] necroptosis,[2-5] autophagy,[6-10] and pyroptosis.[11] A simple time-delay model is included that sacrifices shoulder region information in order to obtain an accurate prediction of later stage cell death — the dying cell fraction is not over-estimated with this method, as it would be if an appropriate time delay was not included.

Damage processes modeled as first-order rate of formation processes require two experimentally derived coefficients. Thermal damage in this formulation is exponentially dependent on temperature and linearly dependent on time of exposure. The rate process models apply well to the prediction of damage thresholds, and less well as the damage becomes complete since several of the fundamental assumptions are violated. The original studies on the application of rate process models to thermal damage were reported by Moritz and Henriques in a series of seminal papers entitled "Studies of Thermal Injury" in 1947.[12-15] In their work, the damage was quantified using a single parameter, Ω, which ranges on the entire positive real axis and is calculated from an Arrhenius integral:

$$\Omega(\tau) = \int_0^{\tau} A\, e^{\left[\frac{-E_a}{R\,T(t)}\right]}\, dt \qquad (1)$$

where: A is a frequency factor (s^{-1}), τ the total heating time (s), E_a an activation energy barrier (J/mole), R the universal gas constant (8.3143 J/mole/K), and T the absolute temperature (K). One difficulty with this description is that a single damage parameter inherently lumps all damage processes into one global measure, so in multiple process cases, the lowest temperature process saturates the damage measure early during heating. In this discussion we review the underlying assumptions and origin of the terms in equation (1) and recast the traditional thermal damage parameter, Ω, into a form suitable for evaluation of multiple-process thermal damage effects and for comparison between numerical models and histologic results.

A. Chemical Reaction Kinetics.

This section briefly reviews the physical chemistry basis for kinetic models of tissue thermal damage. The reaction kinetics formulation is derived from experiment, and has its origins in the experimental work of Svanté Arrhenius in 1889.[16] This work represents a founding pillar of physical chemistry and is worthy of great respect. Prior to Arrhenius' observations, strictly thermodynamic approaches assumed that equilibrium conditions pertained during transformation processes. Kinetic analysis, as he introduced, describes the rate at which thermal processes occur, a non-equilibrium description. The original German language publication is well explained by Johnson, Eyring and Stover in their 1974 book.[17] Briefly, Arrhenius' experiments on reaction velocity showed a temperature dependence that could not be explained by the relative thermal energies of the reactants. The relative reaction velocities were fit by:

$$\frac{k\big|_{T_2}}{k\big|_{T_1}} = e^{\frac{\mu(T_2 - T_1)}{2\,T_2 T_1}} = \left[e^{\frac{\mu}{2\,T_2 T_1}} \right]^{(T_2 - T_1)} = \left[e^{\frac{E_a}{R\,T_2 T_1}} \right]^{(T_2 - T_1)} \qquad (2)$$

where: k = the reaction velocity (s^{-1}) at absolute temperatures T_1 and T_2 (K), and μ is the fit parameter (dimensionless) as originally used by Arrhenius.[18]

The fit parameter was subsequently determined by Henry Eyring and co-workers[19-21] to consist of the "activation energy", E_a (J $mole^{-1}$), divided by the universal gas constant, R = 8.3143 (J $mole^{-1}$ K^{-1}), $\mu/2 = E_a/R$. Equation (2) comprises the "Theory of Relative Reaction Rates", a form of which is the basis for the "Cumulative Equivalent Minutes" assessment method employed in hyperthermia studies. We will revisit this formulation in a later section of these notes.

Table 1. Selected kinetic coefficients, μ, for the theory of relative reaction rates, equation (2).[18]

Process	Fit Coefficient μ
Spontaneous Destruction	
Dibromsuccinic acid	22,200
Compound haemolysin	198,500
Rennet, 2%	90,000
Pepsin, 2%	75,600
Trypsin, 2%	62,000
Emulsin, 0.5%	45,000
Invertase, from yeast	72,000
Digestion	
Casein by trypsin	37,500
Powdered casein by trypsin	7,400
Egg white by pepsin	15,570
Emulsion of egg yolk by pancreatic juice	13,600
Coagulation, Precipitation	
Egg white by heat	135,600
Egg white by sulphuric acid	11,000
Haemoglobin by heat	60,100
Haemolysis by heat	64,000
Haemolysis in the presence of acids, bases and lysins	25,000 to 30,000
Milk by rennet	20,650
Killing	
Bacillus typhosus	92,000
Bacillus paratyphosus in phenol	48,600

1. Two-component Reactions

The concept of an activation energy barrier between reactants and products was introduced by Eyring to provide a physical basis for reaction kinetics.[17] Several of the experimentally determined values for $\mu/2 = E_a/R$ are listed in Table 1.[18] The basis for rate process models of thermal damage may be obtained from chemical reaction kinetics. In a typical irreversible reaction process, thermally active reactants surmount an "activation" energy barrier to form products, as illustrated in Figure 1. In the figure, ΔH^* is the energy barrier, and is essentially equal to E_a in equation (1).

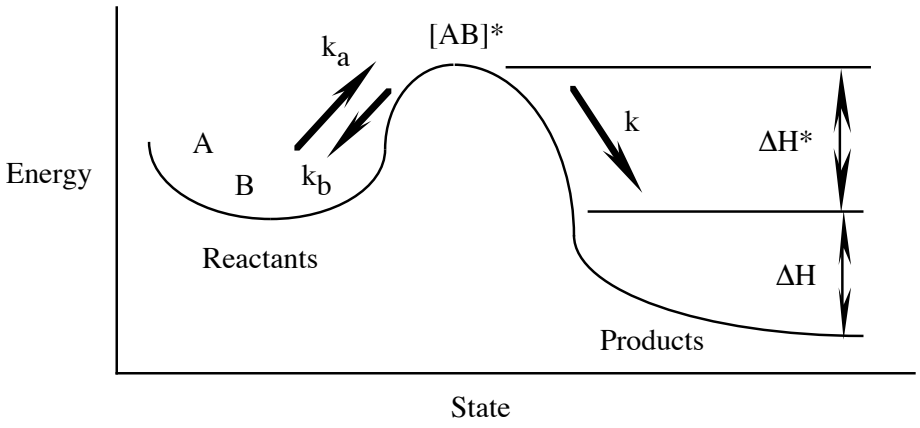

Figure 1 Transition from reactants to products over a reaction energy barrier, ΔH*. The activation energy barrier, ΔH*, should not be confused with the reaction energy, ΔH.

The collision theory description of ordinary first order bi-molecular reaction kinetics (see any physical chemistry text, for example [22]) holds that the reactants are activated by collisions; n* are activated out of n total molecules, and the probability of activation is:

$$\frac{n^*}{n} = e^{\left[\frac{-\Delta G^*}{RT}\right]} \tag{3}$$

where: ΔG* is the Gibb's free energy of activation (J/mole). The Gibb's free energy is one component of the enthalpy of activation, ΔH* (*i.e.* the total activation energy):

$$\Delta H^* = \Delta G^* + T\Delta S^* \tag{4}$$

and the temperature is in (K), while S* is the activation entropy. The activation energy will figure prominently in the description of intrinsic cell death processes in the concluding section.

In such a process, activated reactants are considered to form an activated "complex" which may either relax to inactivated single reactants or progress to form product molecules. The complex has some of the properties of an ordinary molecule, and is at least temporarily stable. For reactant molecules A and B the activated complex is [AB]*, and the sequence of formation is:

$$\text{Reactants} \quad A + B \underset{k_b}{\overset{k_a}{\rightleftarrows}} [AB]^* \xrightarrow{k} \text{Products} \tag{5}$$

where the various "k" are reaction velocities, referring to Figure 1.

The overall reaction velocity, k (s^{-1}), determines the rate of formation of product and is related to the equilibrium constant for formation of the activated complex, K*, by:

$$k = \frac{RT}{N_A h_P} K^* \qquad \text{with:} \qquad K^* = e^{\frac{-\Delta G^*}{RT}} \tag{6}$$

where: N_A is Avogadro's number (6.023×10^{23}), h_P is Planck's constant (6.627×10^{-34} J-s), and ΔG^* is the Gibb's free energy of formation of activated complex (J/mole).

The Gibb's free energy of formation is given by:

$$\Delta G^* = \Delta H^* - T\Delta S^* \tag{7}$$

where: ΔH^* is the enthalpy of activation (J/mole) and ΔS^* is the entropy of activation (J/mole-K) — that is, the entire activation energy (enthalpy) has two parts: the Gibb's free energy of formation and the entropy of activation. The activation entropy is not calculable except for the simplest possible reactions in rarified gases, and is therefore usually determined from experimental measurements of the reaction velocity and activation enthalpy. The activation enthalpy, ΔH^*, is determined from the observed activation energy, E_a by:

$$\Delta H^* = E_a - i\,RT \tag{8}$$

where: i = 1 for first-order reactions in solution and gases, 2 for second order, and 3 for third order reactions. Thermal damage process models are first-order, and E_a is usually >> RT (an example calculation to illustrate this will be presented later).

2. Uni-molecular Process Descriptions

Thermal damage in structural proteins in tissue is a uni-molecular process — tissue constituents (proteins) transition from the native state to the damaged state. Absolute reaction rate theory can be used to explain the rate of formation for a uni-molecular process if we assume that a time lag exists between molecular activation and denaturation.[22] During this time lag, the molecules may either denature or relax back to the native state, as illustrated in Figure 2. Here, ΔH is the enthalpy (energy) difference between native state and denatured molecules. The relative barriers are such that in the thermal damage of tissue, ΔH^*, is almost always smaller than ΔH. So, at temperature the activation process may be regarded as reasonably likely, and the probability of denatured tissue relaxing back to native state tissue is near enough to zero that it may be regarded as the impossible event in the absence of an energy-consuming healing process.

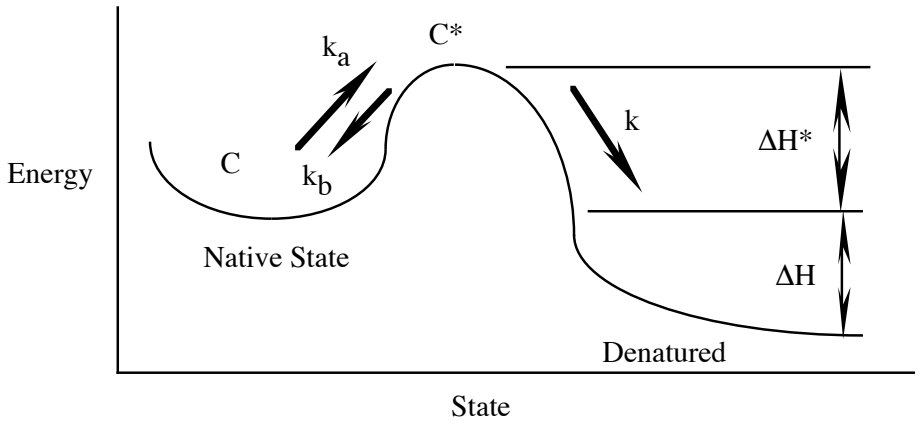

Figure 2 Transition from native state to damaged molecules over an energy barrier, ΔH*.

The rate of damage formation is then proportional to only those molecules that remain activated. For a uni-molecular process in the native state C, having an activated state, C*, with velocity constants k_a, k_b, and k_3:

$$C + C \underset{k_b}{\overset{k_a}{\rightleftharpoons}} C + C^* \tag{9a}$$

$$C^* \xrightarrow{k_3} \text{Damaged Molecules} \tag{9b}$$

The final reaction is essentially a single-step irreversible process, and the rate of disappearance of native state molecules, [C], is given by:

$$-\frac{d[C]}{dt} = k_3 \left[C^*\right] \tag{10}$$

where the bracket is used to indicate molar concentration. Generally [C*] is neither known nor calculable; however, at sufficiently low concentrations of C* the steady state principle asserts that for short-lived activated states the rate of formation can be considered equal to the rate of disappearance. So the activated state, [C*], forms at a rate $k_a [C]^2$, relaxes back to inactivated at rate $k_b [C] [C^*]$, and denatures at rate $k_3 [C^*]$. Consequently:

$$k_a [C]^2 = k_b [C]\left[C^*\right] + k_3\left[C^*\right] \tag{11a}$$

$$\left[C^*\right] = \frac{k_a [C]^2}{k_b [C] + k_3} \tag{11b}$$

We need an overall reaction velocity, k, which relates [C] to its rate of disappearance:

$$-\frac{d[C]}{dt} = k\,[C] \tag{12}$$

There are two limiting cases for equation (11b). First, the concentration of remaining undamaged material, [C], may be large enough that deactivation at k_b dominates the k_3 pathway, so $[C^*] \cong [C]\ k_a/k_b$ for which the overall formation rate, $k = k_3\ (k_a/k_b)$ and a first order process results. Second, if the remaining undamaged material concentration, [C], is small, $k_3 >> k_b\ [C]$ and the process is second order since from equation (11a) $k \cong k_a/k_3\ [C]$. In liquid phase systems with appreciable concentrations of native state molecules the first condition should apply, so the first order approximation generally applies. After a long time of exposure at damaging temperatures such that [C] is very small, $k_3 >> k_b\ [C]$ and a second order process results:

$$-\frac{d[C]}{dt} = k\,[C]^2 \tag{13}$$

where for simplicity the [C] dependence has been removed from k: $k \cong k_a/k_3$. At such low concentrations the damage process is saturated (*i.e.* "complete" for practical purposes), so we may ignore that case for the present.

Equation (12), then, is a Bernoulli differential equation with the solution:

$$C(\tau) = C(0)\,e^{\left\{-\int_0^\tau k\,dt\right\}} \tag{14}$$

Equations (6) and (7) may be used to relate k to ΔH^* and ΔS^*. It should be noted at this point that the energy barrier, E_a, (Figure 1) is in fact $\Delta H^* + RT$ (equation 8); however, in practice $\{\Delta H^* \cong 5 \times 10^5\} >> \{RT \cong 3 \times 10^3\}$, so little error results from assuming that $E_a \cong \Delta H^*$. This approximation may be used to obtain the Eyring-Polyani equation: [20, 23]:

$$k = \left(\frac{RT}{Nh_P}\right)\ e^{\left[\frac{\Delta S^*}{R}+1\right]}\ e^{\left[\frac{-E_a}{RT}\right]} \cong \left(\frac{RT}{Nh_P}\right)\ e^{\left[\frac{\Delta S^*}{R}\right]}\ e^{\left[\frac{-\Delta H^*}{RT}\right]} \tag{15a}$$

$$k \cong A\,e^{\left[\frac{-\Delta H^*}{RT}\right]} \tag{15b}$$

The first term on the left hand side of equation (15a) suggests that the pre-exponential factor, A, is not constant but is in fact temperature-dependent. However, the linear dependence of A on absolute temperature is extremely weak when compared to the exponential-hyperbolic dependence in the final term — and its effect is essentially negligible — so for all practical purposes A may be treated as approximately constant.

B. Arrhenius Models for Thermal Damage Processes.

A more useful form of equation (1) may obtained by recasting the result into a volume fraction model. In this formulation, as above, C signifies the remaining concentration of native state (undamaged) tissue constituent molecules. Therefore, the physical significance of the traditional damage measure, Ω, is the logarithm of the ratio of the original concentration of native tissue to the remaining native state tissue at time τ:

$$\Omega(\tau) = ln\left\{\frac{C(0)}{C(\tau)}\right\} = \int_0^\tau A\, e^{\left[\frac{-E_a}{R\ T(t)}\right]}\, dt \tag{16}$$

where the frequency factor, A, and energy barrier, E_a, are related to the activation enthalpy and entropy, ΔH^* and ΔS^*, by equation (15a).

This form of the damage integral has the advantage that it is easily compared to quantitative pathologic and histologic endpoints such as birefringence loss, collagen damage, or cell survival in culture. Using this description, direct comparisons can be made between the measured histologic damage and computer models of transient thermal fields, T(x, y, z, t) integrated over time. A set of coefficients, A and $E_a \cong \Delta H^*$, is required for each damage process considered in the computer model. Each damage process is then allowed to progress in parallel, driven by the calculated thermal field. This formulation assumes that the individual processes are thermodynamically independent, a reasonable description for most identifiable thermal damage processes. The concentration of each of the damage markers, $C(\tau)_i$, is accumulated; and a distributed field description of the predicted histologic endpoint is generated. The model predictions are then suitable for comparison to histologic results.

For tissue damage processes studied to date A varies from about 10^{40} to 10^{105} (s^{-1}) while E_a ranges from about 1 to 9×10^5 (J/mole); but they are not independent! In their landmark 1939 paper Eyring and Stearn [24] observed that the activation entropy, $\Delta S^* = (\Delta H^* - \Delta G^*)/T$, varied over a relatively small range in the food processing enzymes that they studied, thus the parameters should be approximately linearly related. In 1971 Rosenberg *et al* identified the relationship between ΔH^* and ΔS^* as Compensation Law behavior.[25] In 2003 two seminal papers appeared, one by Xiaoming He and John Bischof [26] and the other by Neil Wright [27] that demonstrated the strikingly linear relationship between $ln\{A\}$ and E_a (J $mole^{-1}$) for multiple thermal damage processes studied to date. Wright used a "polymer in a box" construct originally presented by Miles and Ghelashvili [28] to support the linear relationship hypothesis, and obtained the following fit line for multiple thermal damage process reports:

$$ln\{A\} = 3.832 \times 10^{-4}\ E_a - 10.042 \tag{17a}$$

where E_a is in (J/mole). Nearly simultaneously in 2003, He and Bischof [29], reported a very similar correlation for a much wider range of Arrhenius process damage coefficients:

$$ln\{A\} = 3.800 \times 10^{-4}\ E_a - 9.36 \qquad (17b)$$

Either linear correlation may be used to provide estimates of $ln\{A\}$ for the many reports that contain only the process energy, E_a, or as a sort of "sanity check" for experimentally-derived coefficients.

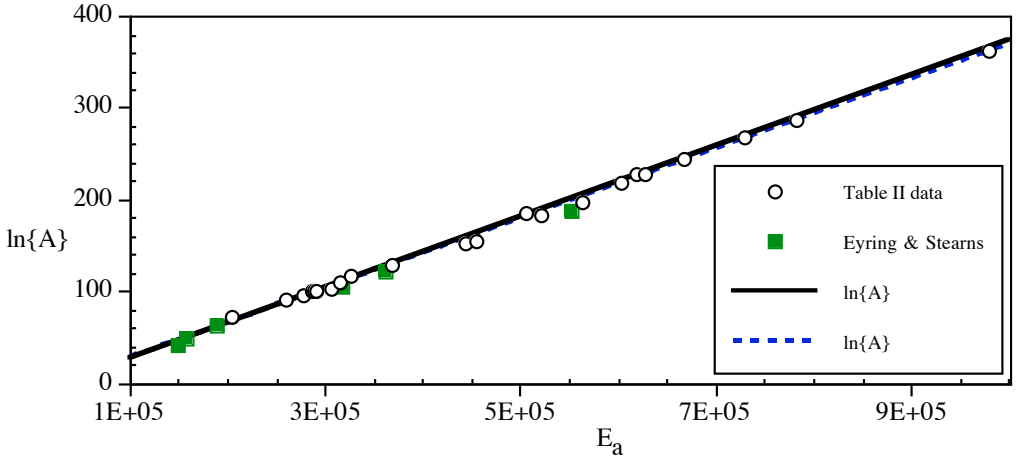

Figure 3 Plot of coefficients from Table 2 (circles) and Eyring and Stearns' enzyme measurements (squares) compared to Eqs. (17a) (solid line) and (17b) (dashed line, barely distinguishable).[30]

1. Functional Behavior of the Damage Model at Constant Temperatures.

The characteristic behavior of the kinetic damage model is that below a threshold temperature the rate of damage accumulation is negligible, and it increases precipitously when this value is exceeded. This behavior is to be expected from the exponential-hyperbolic nature of the function. For purposes of discussion it is useful to define the critical temperature as the temperature at which the damage accumulation rate, $d\Omega/dt$, is 1:

$$\frac{d\Omega}{dt} = 1 = A\ e^{\left[\frac{-E_a}{R\ T_{crit}}\right]} \qquad \text{so,} \qquad T_{crit} = \frac{E_a}{R\ ln\{A\}} \qquad (18)$$

For an arbitrary example process at about the mid-range with representative coefficients of $E_a = 5 \times 10^5$ (J/mole) and $A = 2.825 \times 10^{78}$ ($\ln\{A\} = 180.64$) derived from Eq. (17), the critical temperature is 59.8 C. Figure 4 illustrates the damage accumulation rate dependence on temperature for this example process.

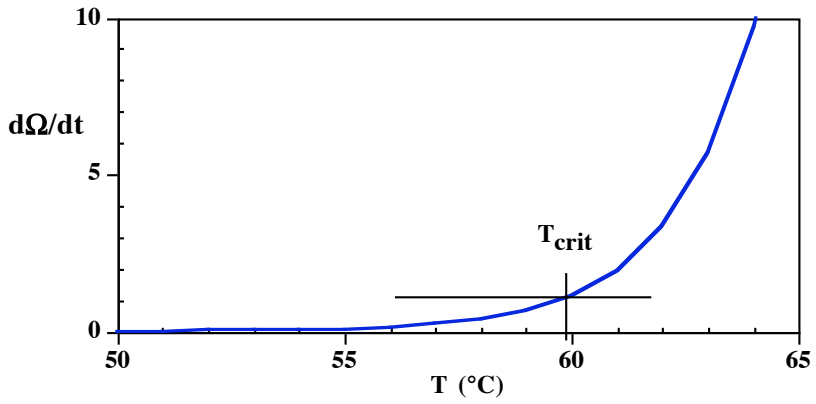

Figure 4 Damage rate, dΩ/dt, *vs* T for process coefficients A = 2.825× 10^{78} and $E_a = 5 \times 10^5$.

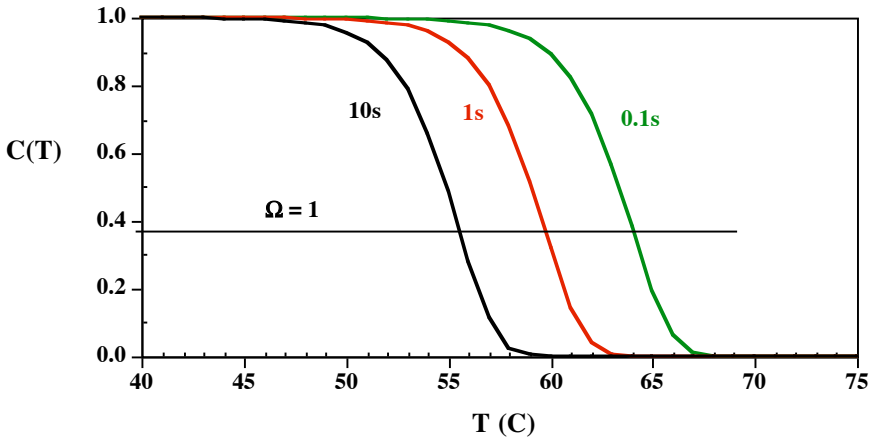

Figure 5 Remaining undamaged tissue vs T for the hypothetical process at different exposure times.

Constant temperature exposures of the example process will result in a decrease in concentration of native state material depending on the time of exposure. Figure 5 shows the remaining concentration for this process for constant temperature exposures of time τ = 0.1, 1.0, and 10 s. The undamaged constituent concentration may be seen to gradually decrease with increasing temperature for fixed exposure times, as expected; the strong exponential nature of the process is evident as well.

2. Determining Arrhenius Process Parameters from Constant Temperature Experiments.

Thermal damage kinetic coefficients are usually determined from constant temperature exposures over a wide range of exposure times. It can be seen from the functional form that several orders of magnitude in exposure times correspond to a relatively narrow range of temperatures. In one approach "threshold" damage results (Ω = 1 or C(τ) = 36.8% of C(0)) are selected out of a set of damaged tissue samples for analysis from a plot like Figure 5 to determine

estimates of A and E_a. If the temperature is held constant at T (K), the integral reduces to a simple multiplication, and $C(\tau) = 0.368\ C(0)$ then equation (16) becomes:

$$ln\{\tau\} = \left(\frac{E_a}{R}\right)\frac{1}{T} - ln\{A\} \tag{19a}$$

If the experimental result does not have $\Omega = 1$, then an estimate of an equivalent exposure time, τ_{eq}, for an experiment in which $\Omega = 1$ would result can be obtained from:

$$ln\left\{\tau_{eq}\right\} = ln\{\tau\} - ln\{\Omega\} = ln\left\{\frac{\tau}{\Omega}\right\} = \left(\frac{E_a}{R}\right)\frac{1}{T} - ln\{A\} \tag{19b}$$

Using this approach, all of the experiments in an ensemble can be corrected to equivalent time and temperature experiments for which $\Omega = 1$. However, this is a very "noisy" approach, usually resulting in substantial uncertainty in the results and low correlation to a linear regression line.

The most effective approach is to calculate reaction velocities, k, from the slope of C(t) plots on log-linear axes. Remember that for constant temperature experiments:

$$k = A\, e^{\left[\frac{-E_a}{R\,T}\right]} \qquad \text{and} \qquad C(t) = e^{[-kt]} \tag{20a}$$

and a constant temperature experiment has a slope of k on a log axis. So, for each experiment temperature, a plot of C(t) has a slope of k. Determine k from the slope at each experiment temperature (by linear regression). Then, noting that:

$$ln\{k\} = ln\{A\} - \left(\frac{E_a}{R}\right)\frac{1}{T} \tag{20b}$$

linear regression on a plot on $ln\{k\}$ *vs* $1/T$ yields $ln\{A\}$ and E_a from the slope and intercept. This approach minimizes the uncertainties by applying linear regression twice to determine the result.

The usual experimental method is to expose thin slices of tissue or cultures of cells to constant temperature in a water bath,[31] by surface application of heated water [12-15] or on a heated metallic plate for desired time intervals. Table 2 lists rate coefficients obtained in various experiments.

III. Example Thermal Damage Processes

This section begins with example thermal damage processes at high temperature for surgery and ablation and concludes with lower temperature processes for which the simpler single-step Arrhenius irreversible reaction model applies. The complex processes involved in intrinsic cell death mechanisms are reserved for the final pages of the notes.

A. High Temperature Surgery and Ablation Damage Processes.

1. Collagen Shrinkage

Collagen is a ubiquitous tissue structural protein consisting of three left-hand α-helices wound in a rope-like molecular form (Figure 6) with a periodicity of about 68 nm.[32] In the figure a small segment of a typical 300 nm long molecule is shown. The 300 nm molecules spontaneously organize into quarter-staggered microfibrils 20 – 40 nm in diameter and these coalesce into larger diameter collagen fibers *in situ*. There are at least 13 different types of collagen fibers that form the structural scaffolding for all tissues; the most common are Types I, II and III collagen.

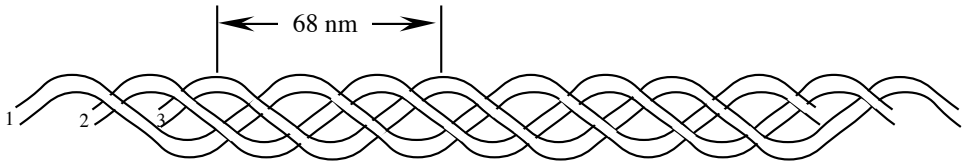

Figure 6. Sketch of periodic structure of the basic collagen molecule. Three of the α-helices intertwine.[33]

Collagen shrinks in length as well as losing its organized regular rope-like arrangement of fibers when heated to sufficient temperatures. This property of collagen is exploited in several radio frequency (RF) cosmetic procedures, and was under investigation as a method to correct hyperopia (far-sightedness). A model for collagen shrinkage obtained by Chen, Wright and Humphrey is a bit different in style from the first order kinetic model, although Arrhenius dependence is built into it.[34-36] They measured shrinkage in rat *chordae tendonae* over several orders of magnitude in time for temperatures between 65 and 90 C and under different applied stresses. They were able to collapse all of their measured data into a single curve, sketched approximately in Figure 7.

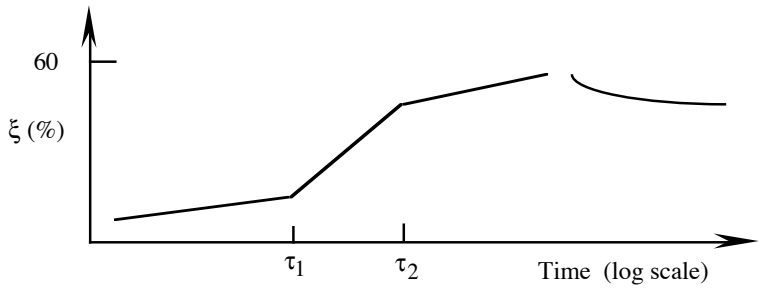

Figure 7. Collagen shrinkage model curve.[37]

In their experiments an initial "slow" shrinkage process (for equivalent exposure time less than τ_1) is followed by a rapid shrinkage period ($\tau_1 < t < \tau_2$) and a final "slow" shrinkage process. The practical maximum for shrinkage in length, ξ (%), is 60%. Longer equivalent exposures result in gellification of the collagen and complete loss of structural properties. Sometimes, however,

gellification is the surgical goal, as in tissue welding applications. After initial shrinkage, the collagen partially relaxes during cooling, indicated by the shrinkage decay region in Figure 7. The curve fit functions utilize a non-dimensional time axis, t/τ_2, where the fit parameters are expressed in the form of the logarithm of the time ratio:

$$\nu = ln\left\{\frac{t}{\tau_2}\right\} \tag{21}$$

The resulting shrinkage is obtained by interpolation between the two slow region curves (through the fast region):

$$\xi = \left(1 - f(\nu)\right)\left[a_0 + a_1 \nu\right] + f(\nu)\left[b_0 + b_1 \nu\right] \tag{22}$$

where: $a_0 = 1.80 \pm 2.25$; $a_1 = 0.983 \pm 0.937$; $b_0 = 42.4 \pm 2.94$; and $b_1 = 3.17 \pm 0.47$ (all in %). The best fit interpolation function, $f(\nu)$, is given by:

$$f(\nu) = \frac{e^{a(\nu - \nu_m)}}{1 + e^{a(\nu - \nu_m)}} \tag{23}$$

where: $a = 2.48 \pm 0.438$, and $\nu_m = \ln\{\tau_1/\tau_2\} = -0.77 \pm 0.26$. Finally, at any temperature τ_2 is given by:

$$\tau_2 = e^{\left[\alpha + \beta P + M/T\right]} \tag{24}$$

where: $\alpha = -152.35$; $\beta = 0.0109$ (kPa^{-1}); P = the applied stress (kPa); and M = 53,256 (K).

The functional form of τ_2 contains the kinetic nature of the process where $\alpha = -ln\{A\} = -152.35$ ($A = 1.461 \times 10^{66}$), and $M = E_a/R$, *i.e.* $E_a = 4.427 \times 10^5$ (J/mole). However, the expression is in the form of an exposure time, rather than a rate of formation as was used in equation 16, and so the coefficient, M, is positive and α is negative. The process has a critical temperature of 76.3 C. To use the collagen shrinkage model, the shrinkage is referred to an equivalent τ_2. That is, at each point in space and time an equivalent value for the increment in t/τ_2 is calculated and accumulated until shrinkage is calculated.

2. Birefringence Loss in Collagen

Native state collagen *in situ* is birefringent; that is, it has the ability to rotate the polarization of a polarized beam of light. One useful measure of irreversible thermal alteration in collagen is that when heated for sufficient time to temperatures in excess of about 60 C the regularity of the fiber array is disrupted and collagen loses its birefringence property (see Figure 8). Transmission

Polarizing Light Microscopy (TPM) is used to image birefringence loss. When viewed through the analyzer, undamaged collagen shows up as a bright field due to its birefringence properties. Thermally damaged collagen loses this property and is dark in the field. The kinetic coefficients for collagen birefringence loss in rat skin are: $A = 1.606 \times 10^{45}$ (s^{-1}) — $ln\{A\} = 104.09$ — and $E_a = 3.06 \times 10^5$ (J/mole).[31] The birefringence-loss damage process in collagen has a critical temperature of 80 C. These coefficients have proven useful over a wide range of heating times from ms to hours.

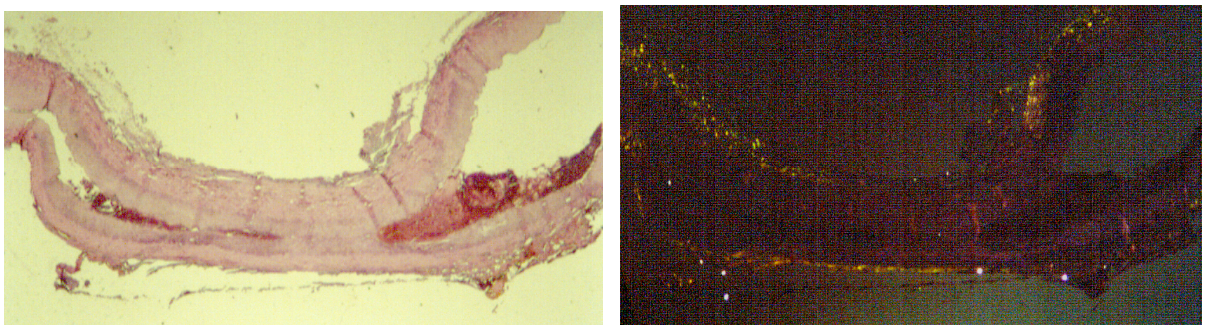

(a) (b)

Figure 8. Vessel collagen birefringence loss under bipolar RF heating. (a) Thermally fused canine carotid artery, H&E stain (Original magnification 40X). (b) TPM view of same section showing loss of birefringence in adventitial collagen under the bipolar plate electrodes.

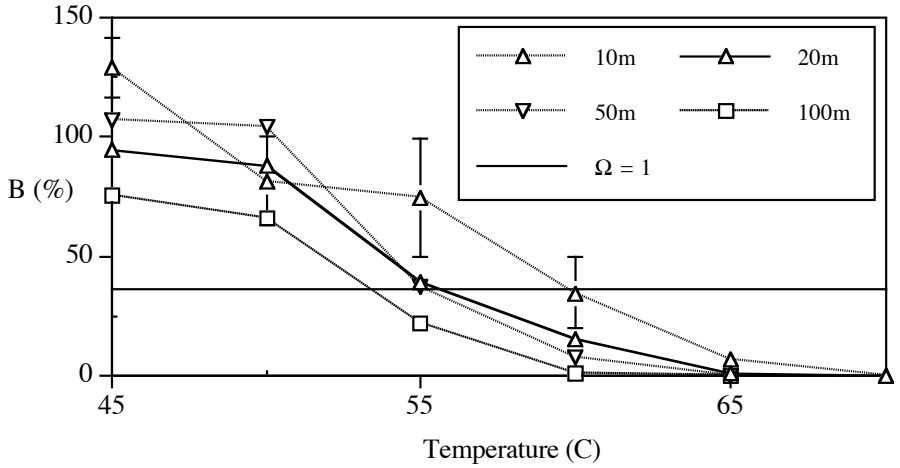

Figure 9 Birefringence loss data plot to estimate A and E_a for different temperature-time combinations.[31] Heating times are given in minutes.

Birefringence loss in rat skin collagen was measured at temperatures between 40 and 90 C in 5 C increments for times ranging from 120 to 6000s.[31] The relative intensity of birefringence was determined using the exposure meter on the microscope camera in the "spot" mode: assuming that reciprocity applies, the intensity is the inverse of the indicated exposure time. Intensity was calculated from data normalized by the background light intensity for each microscope slide, I_0. Relative birefringence intensity was then calculated by subtracting the fully denatured

birefringence intensity, I_d, from the specimen intensity, I_s, and native state (undamaged) intensity, I_n, with all intensities individually normalized by I_0 before the calculation:

$$B = \frac{I_s - I_d}{I_n - I_d} \tag{25}$$

The Ω=1 values were determined from the plot in Figure 9 (similar to Figure 5) to calculate A and E_a. In that figure, data for 10 to 100 minutes of exposure are plotted at six temperatures (error bars = standard deviation for the 10 minute data are provided for comparison purposes). The results have proven very useful despite the uncertainty inherent with this method of extracting the Arrhenius parameters.

B. Lower Temperature Coagulation.

1. Retinal Damage

The measurements of Welch and Polhamus [38] used the diameter of the edge of the visible lesion formed in bovine retina under argon laser irradiation as the damage end point. The temperatures were not measured directly, but were determined in separate experiments on retinas in which a correlation between temperature and radius was established using micro-thermocouples (about 5 μm in diameter) advanced from the posterior surface of the eye to a point just below the retina. The correlates were used to estimate the retinal temperature given laser beam power and duration. The critical temperature for these coefficients is 56.6 C. Takata[39] used a similar decision criterion for retinal damage for shorter exposure times. He fit the data with three sets of coefficients because a single first order model was not sufficient. It would appear that several parallel damage processes were at work in the study, thus a set of coefficients was required. The critical temperature for the high temperature set of coefficients is 59.9 °C. Birngruber *et al* [40] estimated the frequency factor and activation energy from consideration of the thermodynamics of protein and enzyme denaturation processes. Their estimates have a critical temperature of 74.5 C.

2. Birefringence Loss in Myocardium.

Native state muscle, cardiac, skeletal and smooth, is birefringent; this is the source of the histologically identifiable "A-band" (anisotropic band) in the sarcomere of skeletal and cardiac muscle and has its origins in the regularity of the actin-myosin array. Thermally damaged muscle loses this property due to disruption in the actin-myosin array — a marker of substantial structural and functional damage in the sarcomere.[41] As a result, easily identifiable boundaries of thermal damage, and gradation in relative intensity directly comparable to $C(\tau)/C(0)$, can be identified in histologic section through transmission polarizing microscopy, TPM (see Fig. 10). In a good histologic section one can measure the relative intensity of the birefringence signal, which makes a quantitative thermal damage assay amenable to damage fraction calculation. The zone of

birefringence loss corresponds approximately to the grossly observable whitened zone in an acute myocardial lesion, for which Jacques and Gaeeni provide an estimate of kinetic parameters.[42]

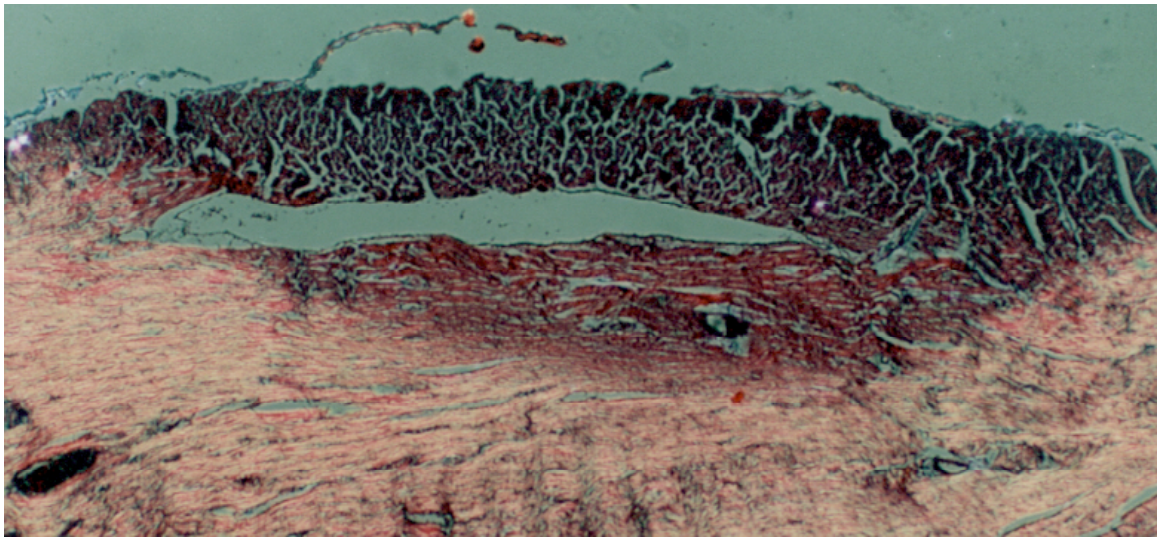

Figure 10 Birefringence loss in rabbit myocardium due to Argon laser irradiation, spot size ~ 2 mm dia. Mallory's trichrome stain, transmission polarizing microscopy (TPM) view; original magnification 40X.

3. Skin Burns.

The end point for $\Omega = 1$ in the original studies of Henriques and Moritz corresponded to a continuum of cascaded effects. In their study the skin of pigs was exposed, *in vivo*, to flowing water at a controlled temperature for exposure times varying over several orders of magnitude. They calibrated their coefficients so that $\Omega = 0.53$ corresponded to the onset of erythema (characterized as "first degree" in their paper). Then $\Omega = 10$ corresponded to a "second degree", or a partial thickness, burn, and $\Omega = 10^4$ to a full thickness, or "third degree", burn. Their coefficients, $A = 3.1 \times 10^{98}$ and $E_a = 6.28 \times 10^5$, have a critical temperature of 59.7 C. Interestingly, although these coefficients have been used for many years, they do not fit their original data very well. In a later analysis, Diller and Klutke applied linear regression to their original data for temperatures less than 52 C – for which $A = 1.3 \times 10^{95}$ and $E_a = 6.04 \times 10^5$ – and if the data point at 52 C is included $A = 0.865 \times 10^{95}$ and $E_a = 6.03 \times 10^5$, virtually the same result.[43] In any event, these new coefficients should be used in future work as they fit the original data much better than those published in 1947. It should be borne in mind that in the original studies the calculation of Ω was based on the temperature of the water flowing over the skin surface. Surface skin in pigs and humans consists of the *stratum corneum*, fully desiccated stratified squamous epithelium, and already dead. The actual damage processes occur below the skin surface (in the epidermis and dermis) where the capillary blood vessel network is found. It

turns out that the damage wave front is relatively well predicted by $C(\tau) = 0.85$ to 0.9 — *i.e.* $\Omega = 0.105$ to 0.163.[37]

Weaver and Stoll[44] used similar criteria to the original 1947 studies and applied two sets of coefficients, as in Table 2 (the upper values are applicable above 50 C) to match the experimental data. The critical temperature for their highest temperature coefficient set is 59.4 C.

C. Comparison of the Processes.

The data from all of the investigators in Table 2 were collected with widely varying assays and damage criteria. The processes studied can reasonably be considered as thermodynamically independent. Consequently, a single set of coefficients or a single calculation of one parameter, such as Ω, which has been used indiscriminately for many years, is neither effective nor instructive. Much can be learned by carrying several damage processes in parallel in model work, as the varying kinetics often have a strong role to play. Figure 11 compares the damage development rate of several of the processes in Table 2.

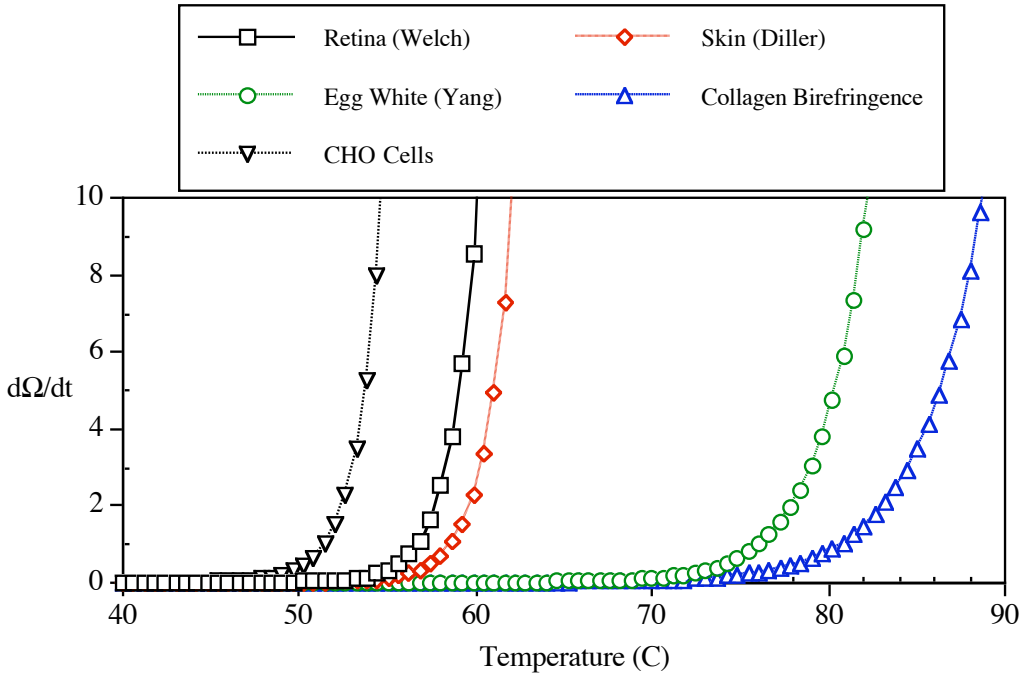

Figure 11 Damage accumulation rates, $d\Omega/dt$, for representative processes from Table 2.

Table 2 Survey of Available Thermal Damage Process Coefficients (Arranged by Damage Type and in the Order of Increasing T_{crit})

Source / Process	Damage Process Coefficients			Notes
	$A\ (s^{-1})$	E_a (J/mole)	T_{crit} (C)	
Heat Shock Proteins				
Beckham [45]	6.90×10^{282}	1.74×10^{6}	48.2	
Skin				
Henriques [13]	3.1×10^{98}	6.28×10^{5}	59.9	Not Recommended
Diller [43]	1.3×10^{95}	6.04×10^{5}	58.5	Recommended
Weaver [44]	2.185×10^{124}	7.82×10^{5}	55.4	$T \leq 50$ C
	1.823×10^{51}	3.27×10^{5}	60.1	$T > 50$ C
Wu [46]	3.1×10^{98}	6.27×10^{5}	59.4	$T \leq 53$ C
	3.1×10^{98}	6.27×10^{5} - 5.1×10^{5} (T-53)	$T > 53$ C	
Fuggitt [47]	3.1×10^{98}	6.28×10^{5}	59.9	$T \leq 55$ C
	5.0×10^{45}	2.96×10^{5}	65.2	$T > 55$ C
Takata [39]	4.322×10^{98}	4.18×10^{5}	64.6	$T \leq 50$ C
	9.39×10^{104}	6.69×10^{5}	59.7	$T > 50$ C
Retinal Damage				
Welch [38]	3.1×10^{99}	6.28×10^{5}	56.6	Damage
Takata [48]	4.322×10^{98}	4.18×10^{5}	64.6	$T \leq 50$ C (Coagulation)
	9.389×10^{104}	6.69×10^{5}	59.7	$T > 50$ C
Vassiliadis [49]	9.95×10^{43}	2.90×10^{5}	71.1	Coagulation
Birngruber [40, 50]	1×10^{44}	2.93×10^{5}	74.7	
Collagen Changes				
Miles [51]	1.60×10^{137}	8.59×10^{5}	53.9	In lens capsule
Jacques [52]	7.35×10^{64}	4.251×10^{5}	69.2	Contraction, Mouse Dermis
Maitland [53]	1.77×10^{56}	3.676×10^{5}	68.2	Rat tail birefringence loss
Pearce [31]	1.606×10^{45}	3.06×10^{5}	80.4	Rat skin birefringence loss
Muscle				
Gaylor [54]	2.9×10^{37}	2.4×10^{5}	61.5	Cell membrane rupture
Jacques [42]	2.94×10^{39}	2.596×10^{5}	70.4	Myocardium Whitening

Erythrocytes				
Moussa [55]	6.8×10^{36}	2.49×10^{5}	80	Membrane denaturation
Lepock [56]	7.6×10^{66}	4.55×10^{5}	82.2	Hemoglobin coagulation
Flock [57]	1×10^{31}	2.12×10^{5}	84	Membrane denaturation
Egg				
Yang [58]	3.8×10^{57}	3.85×10^{5}	76	Egg albumin, whitening
Yang [58]	3.05×10^{56}	3.89×10^{5}	86.6	Egg yolk, whitening
Liver				
Jacques [59]	5.51×10^{41}	2.769×10^{5}	73.4	Whitening, pig
Mathewson [60]	2.09×10^{33}	2.219×10^{5}	74.7	Necrosis, rat liver
Germain [61]	2.688×10^{103}	6.524×10^{5}	56.3	Assumed T, t pairs Not recommeded.
Reddy [62]	2.04×10^{42}*	2.814×10^{5}	73.8	HCC cells
Prostate				
Jacques	2.08×10^{27}	1.866×10^{5}	83.6	Whitening
Skinner [63]	3.8×10^{57}	3.85×10^{5}	76	Whitening, absorption coeff.
Bhowmick [64]	2.99×10^{37}	2.448×10^{5}		AT1 cells, PI
Kidney				
He [65]	1.48×10^{60}	3.996×10^{5}	73.7	Whitening, pig kidney
	3.3×10^{38}	2.569×10^{5}	75.2	Delayed necrosis
Pop [66]	5.73×10^{34}	2.404×10^{5}	88	Electrical conductivity
	5.85×10^{28}	2.023×10^{5}	94.2	Electrical permittivity
He [67]	3.153×10^{47}	3.1493×10^{5}		SN12 cells

* Value for A determined from the He-Bischof equation, (17b).

IV. Cell Survival Curves at Hyperthermic Temperatures

Cell survival curves under the moderate heating, characteristic of hyperthermia treatments — about 40 to 55 C — represent a special case. In the vast majority of cases complex intrinsic mechanisms kill the cells; mechanisms comprised of the complex interactions in systems of functional proteins. The result is that there is often a substantial delay in the development of the death process. Presumably this is time to give the intrinsic repair mechanisms (such as heat shock proteins)[68] — also complex functional protein cascades — a chance to repair the damage due to the thermal stress. Cell survival curves invariably have a slowly developing "shoulder" region in the initial stages of heating. These represent a very special case because the single-step Arrhenius approach fails to represent these survival curves quite miserably. It is just not sufficiently mathematically powerful to accurately represent them. Cell death is invariably over-estimated by an Arrhenius calculation, and an overly optimistic assessment of thermal treatment effectiveness results. This section begins with an overview of cell death assays, includes a development of the "Cumulative Equivalent Minutes at 43 C" parameter as is currently a typically used in hyperthermia work, includes a description of the intricacies of the biochemical systems controlling intrinsic cell death processes, and concludes with a modification to the classical Arrhenius approach from which much more accurate cell death predictions can be obtained.

A. Quantitative Markers of Cell Death.

Fluorescent markers have been used for several decades to indicate thermal processes as they develop. In an early experiment series Green and Diller[69] measured increased macromolecular leakage from capillary vessels in the hamster cheek pouch *in vivo* using flourescein isothiocyanate conjugated dextran (FITC). Heating increased the capillary inter-endothelial cell gaps resulting in increased migration of the dye-tagged dextran into the interstitial space. Aggarwal *et al.*[70] applied digital image processing techniques to measure the diffusion rates of the flourescent labeled dextran in a dorsal skin flap preparation. Bhowmick *et al.*[64] measured the loss of calcein fluorescence in Dunning AT-1 rat prostate tumor cells *in vitro* heated at rates of 2 and 5°C per minute to temperatures between 40 and 70°C. This is the AT-1 subline of the Dunning 3327 rat prostate CA cell line. In an analogous preparation He and Bischof[67] exposed SN12 human renal carcinoma cells to heating rates up to 130°C min^{-1} with varying hold times between 0 and 10 min at hold temperatures between 45 and 70°C followed by a 65°C min^{-1} cooling sequence. The SN12 and AT-1 cell lines were studied for plasma membrane disruption by propidium iodide (PI) uptake. The results for suspended cells differed significantly from those for attached cells (see Table 2), owing to the effects of local stress, and suggest that cellular attachment thermally stabilizes the cells, in some sense. In both of the PI studies a simple Arrhenius model fit the experiment data very effectively. Interestingly, in additional measurements in the AT-1 cells, both the calcein leakage and loss of clonogenicity measurements have a significant shoulder region and a delay time is required to match the data adequately. Clonogenicity is the ability of a CA cell line to continually divide and form new colonies.

The dorsal skin flap is a standard construct that allows continuous close observation of skin vasculature *in vivo* without anesthesia (once implanted) in diverse small animal species.[69] The skin is opened, elevated and clamped between plates supporting removable windows and allowed

to heal. This fixture has been used successfully to study diverse vascular phenomena, including thermal alterations. The thermal breakdown of red blood cells, hemolysis, another primary skin burn response has also been studied with substantial success.

Vital stains are used without fixation to identify viable cells. There are many; a partial list includes: trypan blue, vital red, neutral red, Nile blue, methylene blue, acrydine orange, Bismarck brown and Janus green. Janus green B, for example, has been used to study mitochondria in the cornea[71] and elsewhere. Indocyanine green (ICG) is another common vital stain (and laser chromophore); however, its use in retinal surgery, for example, has recently come under scrutiny due to possible toxic effects.[72] Another interesting supravital stain is Nitro Blue Tetrazolium (NBT), used to study myocardial cell function by Acosta and Wendel in 1975,[73] and by Feldman *et al.*[74] and Lucchesi et al. in 1976,[75] and many others since. NBT stains normal, metabolically active tissue a dark purple/brown color.

B. Deriving Arrhenius Coefficients From Cell Survival Curves

Another format typically used to present thermal damage data is the cell survival curve, derived from cell culture experiments. The simplest format to calculate A and E_a is a plot of surviving fraction *vs.* time at fixed temperature. A typical cell survival curve set is shown in Figure 11, reported by Sapareto *et al.* in 1978.[76-78] The data shown are for asynchronously dividing Chinese Hamster Ovary cells (CHO), a standard tumor cell line. The marker of vitality in this study is the ability of the cells to form colonies, *i.e.* the rate at which that happens. In the plot, there is an initial slowly developing "shoulder" region followed by a constant rate region. The constant rate region is the region from which the time constant D_0 is determined and modeled by both the Arrhenius and CEM formulations. For the constant rate region the surviving fraction, S/N_0, is simply $C(\tau)/C(0)$, and a straight forward calculation can be done for $\Omega(\tau)$, from which A and E_a can quickly be extracted by curve fitting.

1. Fundamental relations.

Placing the relation on a quantitative basis, for a constant temperature exposure at T the constant rate region has:

$$\left.\frac{S}{N_0}\right|_t = e^{-\frac{t-t_0}{D_0(T)}} \tag{26}$$

where: N_0 is determined at time t_0, and the ratio is determined at time t. Note that $t - t_0 = \tau$ the limit of the Arrhenius integral (Equation 1). Figure 13 contains the measured slope data, $D_0(T)$, for both asynchronously dividing and G1 phase CHO cells; at $D_0(T)$ the cell population has decreased by a factor of $e^{-1} = 0.368$. G1 phase cells are resting and not in the process of dividing.

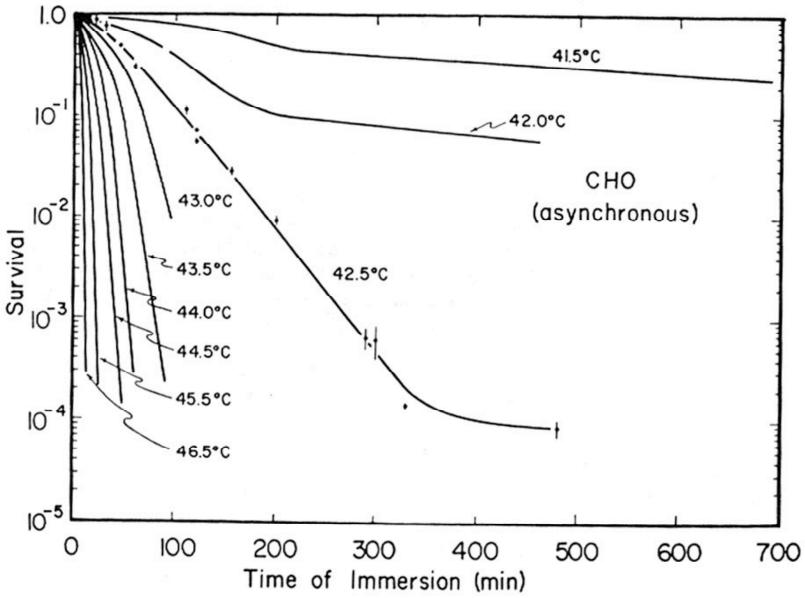

Figure 12 Classical cell survival curves for Chinese Hamster Ovary (CHO) cells as measured by Sapareto *et al* in 1978.[76, 77] The survival curves typically exhibit an initial slow "shoulder" region, followed by a constant rate region and a "foot" at long duration and low temperatures.[78]

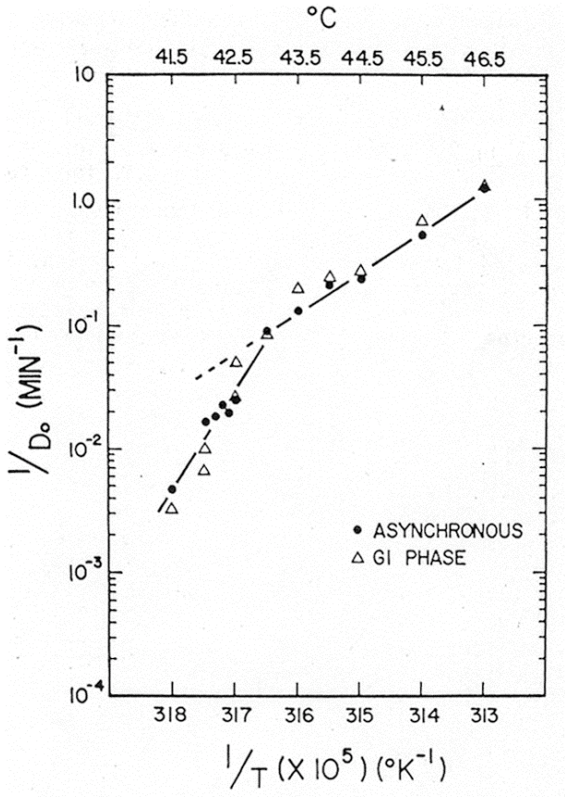

Figure 13 Plot of the constant rate region slopes for CHO cells.[76]

The constant rate region has a total cell death of $(1\text{-}S/N_0)$, so the cell death rate is:

$$\text{Cell Death Rate} = \frac{\partial}{\partial t}\left(1 - e^{-\frac{t-t_0}{D_0(T)}}\right) = \frac{1}{D_0(T)} \tag{27}$$

Consequently, the parameter that is comparable to the Arrhenius formulation is the cell death rate = the rate of disappearance of native state molecules, $k = 1/D_0$.

$$ln\left\{\frac{C(0)}{C(\tau)}\right\} = 1 = \int_0^{D_0} A\, e^{\left[\frac{-E_a}{RT}\right]}\, dt \tag{28}$$

From Eq. (28) it may quickly be determined that:

$$ln\{D_0\} = \frac{E_a}{RT} - ln\{A\} \tag{29}$$

The Arrhenius plot from cell survival data for asynchronous CHO cells above 43 C gives E_a/R = 74417 and $ln\{A\}$ = 229. For the CHO cells in this data set $A = 2.84 \times 10^{99}$ (s^{-1}), $E_a = 6.18 \times 10^5$ (J/mole), and T_{crit} = 51.4 C in the constant rate region. NOTE: this calculation applies in the constant rate region and ignores the shoulder region.

To date, one study has provided kinetic coefficients for combined apoptosis and necrosis, as indicated by 2-3-5 triphenyl tetrazolium chloride (TTC) vital stain studies in excised human prostate.[79] These results are particularly interesting since the low activation energy, $E_a = 1.61 \times 10^5$ (J $mole^{-1}$), and high critical temperature (94.2 °C) indicate a relatively slow process not likely to be observed in relatively rapid heating, such as characterizes electromagnetic and laser sources (Table 2). A recent study by McMillan[80] used nitro-blue tetrazolium (NBT) in tonsil tissue. Several cell death studies have been included in Table 2, but for those that the Arrhenius accurately fits the survival curves. Substantially more in-depth discussion of cell death processes appears in section C of this chapter.

2. Cumulative Equivalent Minutes at 43 C.

The alternate Relative Reaction Rate form of the Arrhenius formulation is typically used in tumor hyperthermia studies. A particular thermal history is compared to an equivalent time of exposure at the apparent breakpoint in the CHO cell curve data, 43 C, using a time scaling ratio, R_{CEM} (to distinguish it from the gas constant). The "Cumulative Equivalent Minutes at 43 C" (CEM_{43}) method is a common formulation for assessing and modeling expected thermal damage in tumor hyperthermia literature: Note that CEM does not have predictive value, but simply compares time of exposure to a standard treatment. The damage levels that represent likely cell death are expressed in terms of the equivalent exposure time at a constant temperature of 43 C, the breakpoint for the CHO cells, and several other relevant cell types.

Recasting equation (3) in terms of the relative reaction times, rather than velocities, gives a time scaling ratio, R_{CEM}:

$$\frac{\tau_2}{\tau_1} = \left[e^{\frac{-E_a}{R\,T_2 T_1}} \right]^{(T_2 - T_1)} = \left[R_{CEM} \right]^{(T_2 - T_1)} \qquad \text{so} \qquad R_{CEM} = e^{\frac{-E_a}{RT_1(T_1+1)}} \tag{30}$$

The equivalent exposure time at the breakpoint temperature, 43 C for the CHO cells, CEM_{43} is calculated from:

$$CEM_{43} = \sum_{i=1}^{N} \left[R_{CEM} \right]^{(43 - T_i)} t_i = \int_0^{\tau} \left[R_{CEM} \right]^{(43 - T)} dt \tag{31}$$

where: the thermal history is either a discrete ensemble, (T_i, t_i), or continuous, as in the integral — here the temperature is in Celsius, and the reference temperature takes the place of T_2 in equation (30). The particular breakpoint at 43 C has been interpreted as the limit at which cell thermal response mechanisms (*i.e.* thermotolerance) can function.[56]

In hyperthermia studies the time scaling ratio is usually set to 0.5 above 43 C and 0.25 below the breakpoint temperature. However, inspection of Table 3, where R_{CEM} has been calculated from Equation (28) reveals that R_{CEM} varies widely for the different cell types, from about 0.3 to 0.83. Inspection of Equations 16, 26 and 29 reveals that, in essence, $\Omega = CEM/D_0(T_{break})$ — however, a useful estimate can only be obtained if the appropriate value of R_{CEM} has been used to calculate CEM. Curve fitting can be used to obtain a fit between CEM and Ω; however, the fit coefficients rarely lie close to $1/D_0(T_{break})$, as would be expected. Also, CEM calculations are based on a constant value for R_{CEM}. Plainly from Equation (30) R_{CEM} is a function of temperature. The error when constant R_{CEM} is used becomes significant about 5 to 7 degrees above the reference temperature. CEM is a comparative measure that relates different temperature histories, and should not be used predictively. CEM is a weak form of the Arrhenius method, and the classical Arrhenius method does not give acceptably accurate results for typical hyperthermic temperature range cell death processes, 43 to 50 C due to the usual shoulder region.

3. Failure of the Arrhenius Model to Represent Cell Survival Curve Data.

Figure 14 illustrates the failure of the single step irreversible Arrhenius model to predict typical survival curve data at hyperthermic temperatures. Typical survival curves, like those for the CHO cells (Figure 12), have a slowly developing shoulder region that the Arrhenius calculation cannot accurately represent.

Table 3 Time scaling ratios, R_{CEM}, calculated from Equation (28) for various cell types.

Process	Process Parameters			Notes
	A (s^{-1})	E_a (J $mole^{-1}$)	R_{CEM} 44C	
Cell Death				
Sapareto [78]	2.84×10^{99}	6.18×10^5	0.477	CHO Cells, T > 43°C
Beckham [45]	6.9×10^{116}	7.3×10^5	0.417	w/o Hsp70 production
	3.7×10^{157}	9.8×10^5	0.309	w/ Hsp70 production
He [29]	2.53×10^{24}	1.684×10^5	0.818	Hu. BPH; EthD
	1.79×10^{23}	1.613×10^5	0.825	BPH; apop., necrosis
Bhowmick [81]	1.66×10^{91}	5.68×10^5	0.506	AT-1 Cells < 50°C
	173.5	1.97×10^4	0.977	AT-1 Cells > 50°C
Borrelli [82]	2.984×10^{80}	5.064×10^5	0.545	BHK Cells
He [67]	4.362×10^{43}	2.875×10^5	0.708	SN12 cells, suspended
	3.153×10^{47}	3.149×10^5	0.685	SN12 cells, attached
Arrhenius [18]	$^{**}2.02 \times 10^{60}$	3.82×10^5	0.635	Bacillus typhosus
Arrhenius [18]	$^{**}9.40 \times 10^{29}$	2.02×10^5	0.786	Bacillus paratyphosus in phenol
Erythrocytes				
Lepock [56]	7.6×10^{66}	4.55×10^5	0.579	Haemolysis
Arrhenius [18]	$^{**}5.72 \times 10^{40}$	2.66×10^5	0.729	Haemolysis
Przybylska [83]	$^{*}1.08 \times 10^{44}$	2.908×10^5	0.705	Hemol. Normal
	$^{*}3.7 \times 10^{43}$	2.88×10^5	0.708	Down's Syndrome
Skin Burns				
Henriques [13]	3.1×10^{98}	6.28×10^5		Not Recommended
Diller [84]	8.82×10^{94}	6.03×10^5	0.485	T ≤ 53°C (same data)
	1.297×10^{31}	2.04×10^5		T > 53°C
Weaver [44]	2.19×10^{124}	7.82×10^5	0.391	T ≤ 50°C
	1.82×10^{51}	3.27×10^5		T > 50°C
Retinal Damage				
Welch [38]	3.1×10^{99}	6.28×10^5	0.471	Whitening

* The value for A has been estimated from Wright's line, Eq. (6.17a).

** The value for A has been estimated from the He-Bischof line, Eq. (6.17b)

Many damage process assays exhibit similar curve shapes, and the Arrhenius calculation always over-predicts the death rate because it begins at t = 0 and is constant-rate. Figure 14 data were extracted from the Bhowmick *et al*. 2000 paper and are plotted here.[64] The exponential decay of the Arrhenius calculation (lines) obviously fails in the early stages of cell heating. We will next look at some representative cell death processes and develop more effective models for mild heating in the hyperthermic range. The biochemistry of these processes in extremely interesting.

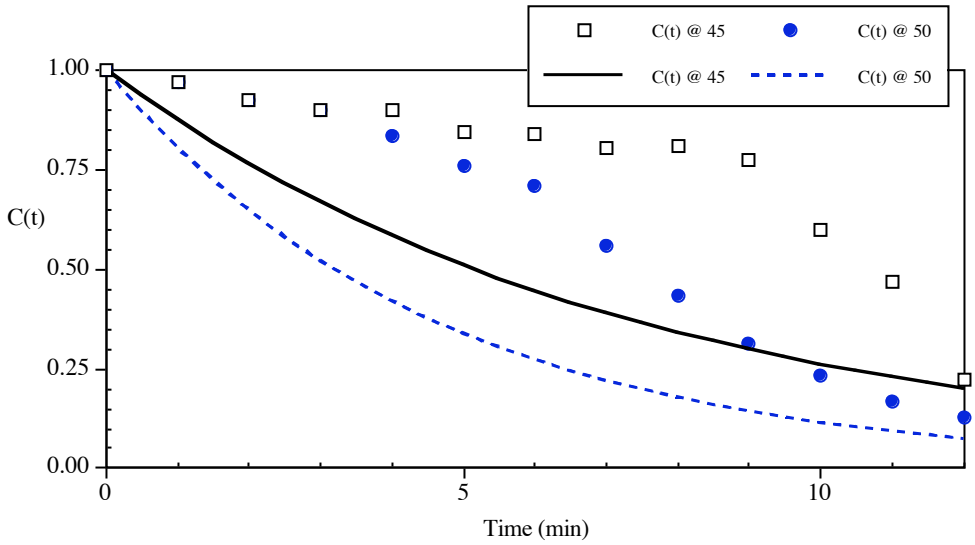

Figure 14 Illustration of one of the failure of Arrhenius predictions to accurately predict cell survival curve data. Plot of calcein fluorescence signal loss in Dunning AT-1 tumor cell studies.[64] Data points were extracted from mean values in Fig. 2 of the publication at temperatures of 45 and 50 C. The Arrhenius fit was based on reported parameters (lines as indicated). In both cases the signal loss is substantially over-predicted except for the longest heating times.

C. Cell Death Processes.

Cell death processes are either intrinsic — in which an internal signal initiates an intricate protein reaction cascade — or extrinsic, in which either a signaling protein ligand initiates the cascade, or a major thermal insult results in structural damage to organelles or other functional cellular inclusions. Intrinsic cell death processes identified to date include: apoptosis, necroptosis, autophagy, and pyroptosis all forms of “Programmed Cell Death” (PCD).[85] PCD, in turn, can result from intrinsic signals (such as when various tissue structures are resorbed during embryonic development) or extrinsic signals (as when tumor necrosis factor, TNF, bind to surface ligand receptor complexes). The resulting protein reaction cascade includes many feedback loops and branch reactions that cannot be well represented by a single constant-rate model, like the Arrhenius model. This is the likely reason for the failure of Arrhenius models to describe the shoulder region in cells survival curves. Description and modeling of these processes belongs to the study of systems biology. A brief description and example are presented here to illustrate the intricacy.

1. Brief Review of The Biology of Apoptosis

Apoptosis (from the Greek meaning "falling off") is perhaps the best understood intrinsic cell death process — there are 10s of thousands of apoptosis references, most of which have appeared within the last 15 years. The apoptosis process is important to all complex organisms as a means to control cell growth and/or embryonic development. It is extremely important in cancer studies, because the ability to avoid apoptosis is one of the hallmarks of cancer. Initiating signals may be

extrinsic, as in the TNF example above, or intrinsic, as in the action of p53, the so-called "guardian of the genome". The hallmark of apoptosis is a cascade of activation reactions in caspase proteins. "Activation" in functional proteins can be simply a matter of slightly changing the protein conformation to expose an active enzyme catalytic site on the long protein molecule. Caspases are cysteine aspartic proteases, and they exist to cleave other proteins when transformed from the inactive "procaspase" state to the activated state — two procaspase molecules lose their N-terminus, and are cleaved to form one activated caspase hetero-tetramer

There are two classes of caspases: initiator caspases (C2, C8, C9 and C10) and executioner caspases (C3, C6 and C7). Activated initiator caspases activate executioner caspases that cleave cytosolic proteins, including structural proteins, like the cytoskeleton. In end-stage apoptosis the plasma membrane collapses into "blebs", or small, enclosed volumes of cellular debris completely enclosed by segments of the plasma membrane. The resulting "apoptotic bodies" are then disposed of by macrophages. In normal cells the membrane protein distribution is highly assymmetrical. In an apoptotic body, the plasma membrane protein "scramblease", which is normally held inactive on the cytosolic leaflet of the plasma membrane, is activated and the plasma membrane proteins assume a random symmetrical distribution, which acts as an "eat me" signal for circulating macrophages. Kind of an environmentally sensitive disposal mechanism, you might say.

The substantial role of mitochondria in these events is also quite important: in addition to their role in energy production they contain and release cytochrome *c* (cyt*C*) and apoptosis inducing factor.[86] Cytochrome *C* — originally named when discovered and incorrectly thought to be a respiratory pigment — is an important link in the electron transport chain (ETC) at the end of the glucose metabolism process that results in adenosine tri-phosphate (ATP) production; ATP is the energy source for many active diffusion processes. Cyt*C* resides on the outer leaflet of the inner membrane of mitochondria and couples the output molecules of ETC complex III to the input of complex IV. Complex IV output is then directly processed by ATP Synthase in the final step of ATP production, producing the largest number of ATP molecules from adenosine di-phosphate (ADP) in oxidative phosphorylation. The ETC maintains a low (acidic) pH in the inter-membrane space of the mitochondria. In end-stage apoptosis, cyt*C* is released and combines with APAF-1 and activated caspase 9 (at the hub) to form an apoptosome, a so-called "wheel of death" that cleaves proteins in the cell, both structural and functional, by activating executioner caspases.

2. Necroptosis, Autophagy and Pyroptosis.

The necroptosis cascade has recently been identified as differentiated from apoptosis in that following the tumor necrosis factor (TNF) - receptor interacting protein (RIP) sequence (TNF-RIP1, RIP3 …), it results from caspase-independent mechanisms.[4, 5] The hallmark of apoptosis is caspase-dependent mechanisms.[85, 87] The final result in necroptosis is direct disintegration of the plasma membrane, releasing degraded cytosolic contents into the extra-cellular space. It has been described as an "ordered explosion" of cells.[5]

Autophagy is an intrinsic cellular process that identifies badly-formed and/or badly-behaved proteins and sequesters them into endosomes, *i.e.* repair enclosures maintained within the cell. Sequestered proteins can be disassembled into subunits and re-used, or if the threat to the cell is

severe enough the endosome can transition into an extremely low pH lysosome for complete destruction. In extreme cases a decision may be made to commit cellular suicide. An excellent review article on the topic of autophagy can be found in the International Journal of Hyperthermia.[10]

Finally, pyroptosis is the result of a pyrogen — a circulating protein that initiates a fever, such as one of the interleukins (Il-1, etc.) A pryroptosis response activates caspase-1.[11] This is not a thermally-induced process, however.

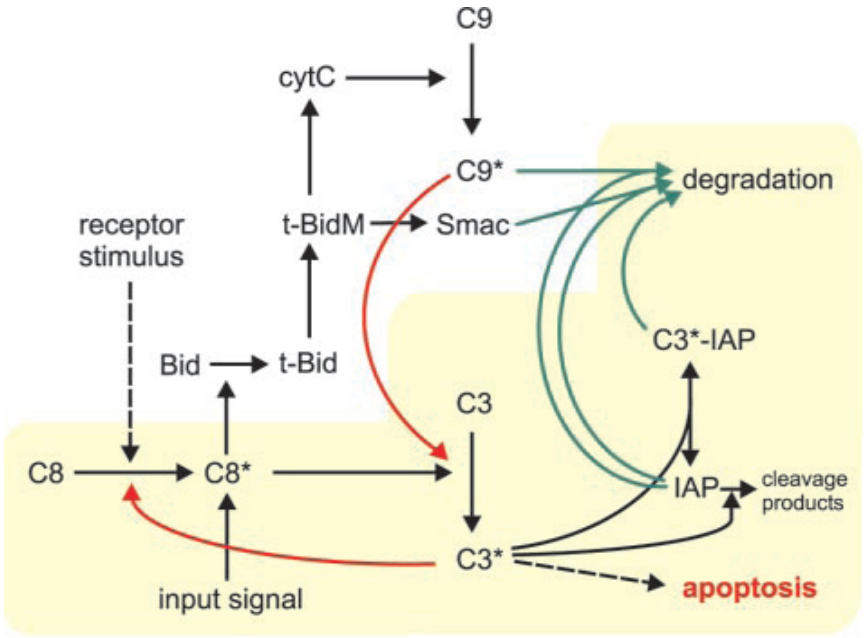

Figure 15 Outline of apoptotic pathways downstream of death receptors signals. Initially, partial activation of caspase 8 (C8*) is mediated by death receptor stimulation. C8* can cleave and activate caspase 3 (C3) directly, but also cleaves Bid to release t-Bid. Mitochondrial t-Bid (t-BidM) leads to the release of cytochrome *c* (cytC) and Smac/DIABLO (Smac). Caspase 9 (C9) is activated by cyt*C* and activates C3. C3* can activate residual C8 in a feedback loop. C9* and C3* can be inhibited by IAP molecules and subsequently fed into proteasomal degradation. Mitochondrially released Smac competes with the caspases for IAP binding and degradation.[88]

3. The Biochemistry of Apoptosis.

An example simplified apoptosis sequence model was presented by Eissing *et al.*[88] The simplified model in Figure 15 of receptor-induced apoptosis (in type I cells) illustrates the complex and intricate nature of these processes. Their model work revealed key aspects of a fast execution phase and bistability — *i.e.* a "switch" mode. The system must be bistable; that is, the "alive" state must be stable against noise unless triggered by a substantial signal, and then must cascade (irreversibly) into a cell death sequence (apoptosis). The authors' results also show how to

reconcile the fast kinetics of caspase 3 activation observed in single cells with the much slower kinetics that describe cell populations.

The biochemical model includes four reactions, one of which is reversible, as in Equations 32 below. C8 represents all of the initiator caspases, and C3 all of the executioner caspases.

$$C8^{*}+C3 \longrightarrow C8^{*}+C3^{*} \tag{32a}$$

$$C8+C3^{*} \longrightarrow C8^{*}+C3^{*} \tag{32b}$$

$$C3^{*}+IAP \longleftrightarrow iC3^{*} \sim IAP \tag{32c}$$

$$C3^{*}+IAP \longrightarrow C3^{*} \tag{32d}$$

These four reactions require 8 state-space system dynamic response relations to describe. The 8-state-equation reaction sequence in this model, although considerably simplified, is also instructive in its complexity (Equations 33).

$$\frac{d[C8]}{dt} = -k_2[C3^{*}][C8] - k_9[C8] + k_{-9} \tag{33a}$$

$$\frac{d[C8^{*}]}{dt} = -k_2[C3^{*}][C8] + k_5[C8^{*}]k_{11}[C8^{*}][BAR] \tag{33b}$$

$$\frac{d[C3]}{dt} = -k_1[C8^{*}][C3] - k_{10}[C3] + k_{-10} \tag{33c}$$

$$\frac{d[C3^{*}]}{dt} = k_1[C8^{*}][C3] - k_3[C3^{*}][IAP] + k_{-3}[iC3^{*} \sim IAP] \tag{33d}$$

$$\frac{d[IAP]}{dt} = -k_3[C3^{*}][IAP] + k_{-3}[iC3^{*} \sim IAP] - k_4[C3^{*}][IAP] - k_8[IAP] + k_{-8} \tag{33e}$$

$$\frac{d[C3 \sim IAP]}{dt} = k_3[C3^{*}][IAP] - k_{-3}[iC3^{*} \sim IAP] - k_7[iC3^{*} \sim IAP] \tag{33f}$$

$$\frac{d[BAR]}{dt} = -k_{11}[C8^{*}][BAR] + k_{-11}[iC8^{*} \sim BAR] - k_{12}[BAR] + k_{-12} \tag{33g}$$

$$\frac{d[C8^* \sim BAR]}{dt} = k_{11}[C8^*][BAR] - k_{-11}[iC8^* \sim BAR] - k_{13}[iC8^* \sim BAR] \qquad (33h)$$

The cleavage reactions (33a, b and d) are considered irreversible and the intermediary cleavage products — "enzyme-substrate complexes" — are assumed to achieve very low levels (to match simulation experiment results). The rate equations come from the laws of mass action. The molecules included in the model are: 1) the caspases (Cx) are proteolytic enzymes that cleave a number of cellular proteins, 2) BAR = Bifunctional Apoptosis Regulators, a family of proteins (examples are the Bcl-2 family of proteins, some of which are apoptosis-promoting, others of which are apoptosis-inhibiting), 3) IAP = Inhibitor of Apoptosis Proteins, 4) tBid is an apoptotic protein, and tBidM originates in the mitochondria, the "t" refers to a truncated protein 5) iCx = inhibited caspases.

The initial conditions for an unstimulated HeLa cell are: 1) C8 = 1.3 x 10^5 molecules/cell, C3 = 2.1 x 10^4 molecules/cell, 2) IAP(s) were estimated to be 4 x 10^4 molecules/cell. Other compounds were not considered to be present in an unstimulated cell. One interesting feature of these reactions is the relatively low value of the reaction velocities in their model, the parameters in Table 4.

Table 4 Model parameters used by Eissing *et al*. to represent the bistable apoptosis cascade.

Parameter	Value	Unit	Parameter	Value	Unit
k_1	5.8×10^{-5}	cell min^{-1} mo^{-1}	k_{-1}	0	
k_2	10^{-5}	cell min^{-1} mo^{-1}	k_{-2}	0	
k_3	5×10^{-4}	cell min^{-1} mo^{-1}	k_{-3}	0.21	min^{-1}
k_4	3×10^{-4}	cell min^{-1} mo^{-1}	k_{-4}	0	
k_5	5.8×10^{-3}	min^{-1}	k_{-5}	0	
k_6	5.8×10^{-3}	min^{-1}	k_{-6}	0	
k_7	1.73×10^{-2}	min^{-1}	k_{-7}	0	
k_8	1.16×10^{-2}	min^{-1}	k_{-8}	464	mo cell min^{-1}
k_9	3.9×10^{-3}	min^{-1}	k_{-9}	507	mo cell min^{-1}
k_{10}	3.9×10^{-3}	min^{-1}	k_{-10}	81.9	mo cell min^{-1}
k_{11}	5×10^{-4}	cell min^{-1} mo^{-1}	k_{-11}	0.21	min^{-1}
k_{12}	10^{-3}	min^{-1}	k_{-12}	40	mo cell min^{-1}
k_{13}	1.16×10^{-2}	min^{-1}	k_{-13}	0	

Systems biologists are actively pursuing these avenues of research due to their wide-spread implications, from auto-immune diseases — glomerulonephritis (kidney failure) and rheumatoid arthritis — to viral assault (HIV, etc.) and aging processes. This will continue to be an important research topic, and is of keen interest in tumor hyperthermia therapy.

The Eissing *et al* paper presents some interesting and instructive results. The numerical model calculations were computed using Copasi, freeware available from the BioInformatics Research Group at Virginia Tech. The plot in Figure 16 shows the delay in the bistable response for two input stimulus levels, 750 activated C8* molecules per cell (delay about 1,300 minutes or 22 hours) and 3,000 molecules per cell (delay approximately 200 minutes, or 3.3 hours). At elevated temperatures the input signal would be thermally-activated C8. The model output illustrates the switching function of the biochemical structure for a single cell.

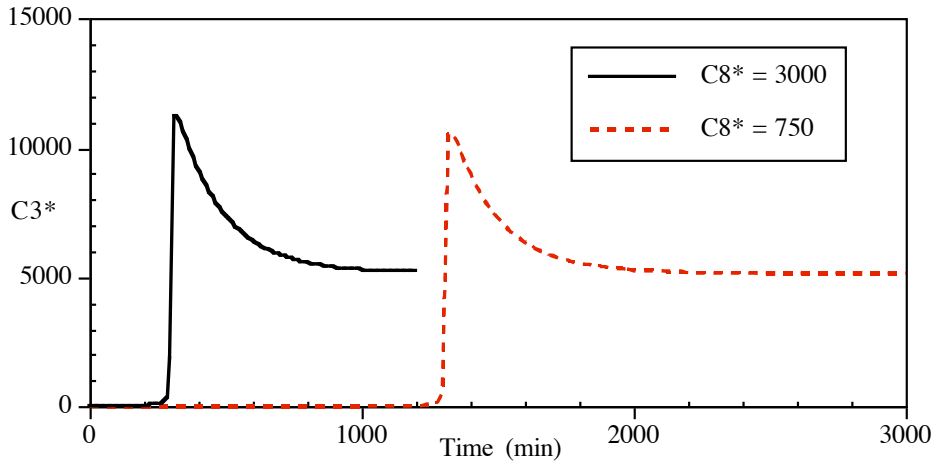

Figure 16 Model calculations of the dynamic response of the C3* output to input signal strengths (C8*) at 750 and 3000 molecules/cell.[30] Copasi 4.8 was used to make the calculations based on a model file kindly provided by Dr. Thomas Eissing.

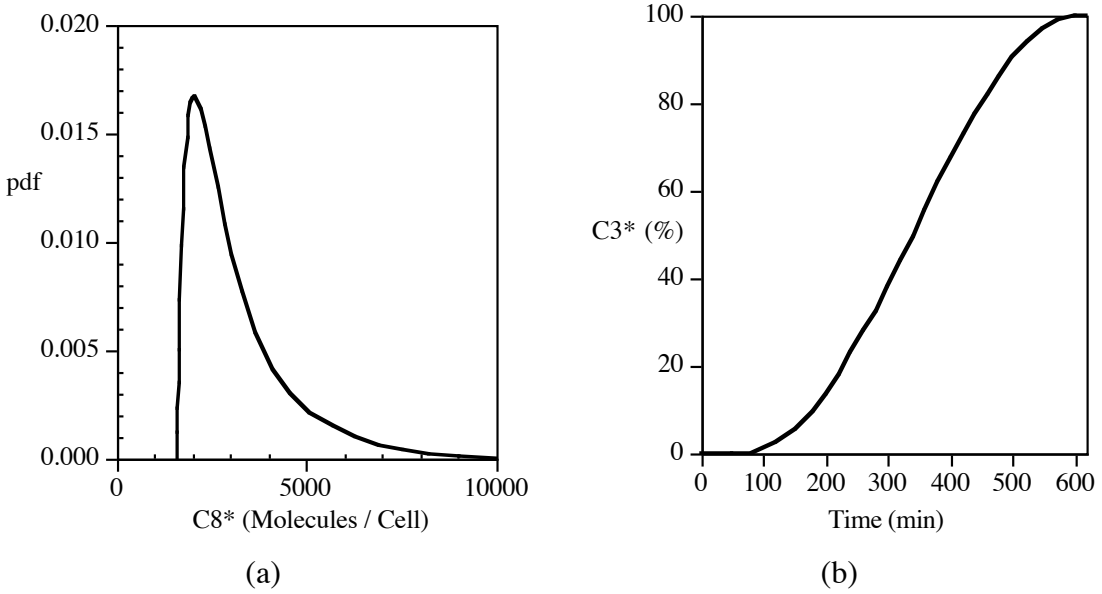

Figure 17 Cell population apoptosis model prediction. a) Probability density function for the C8* input signal to a population of cells. b) The population response in the form of C3* activation.[30]

A population of cells would have some form of probability density function C8 activations. The authors extended their result to a population of cells, as in Figure 21. The important overall message is that a variable delay time is required to effectively model the shoulder region of a survival curve. The delay function most likely comes from association and or dissociation reaction terms, the nonlinear terms in equations 33. A negative term, -k $[C_1]$ $[C_2]$ is an association reaction decreasing the free concentration, and a positive term is a dissociation reaction, increasing the native state concentration.

D. Effective Mathematical Models of Cell Survival Curve Data.

Noting the failure of the standard Arrhenius calculation, several alternative mathematical models have been suggested over the past few decades.

1. Two examples From Literature.

For example, Mackey and Roti Roti applied a probabilistic model to CHO clonogenic cell death (their own data, not the Sapareto & Dewey data) with some success.[89] Their model was heuristically postulated and employed a temperature-dependent parameter, $\varepsilon(T, t)$, to represent the remaining clonogenically active cell population — $\varepsilon(T, t)$ was Gaussian distributed about a mean value, and the steady-state mean value had an Arrhenius term. The model included a delay in the step response of the population mean to approach the steady-state value. The probabilistic model was effective, but as Roti Roti mentioned in a later review paper, it was derived from curve fitting, and not from physical principles.[90]

In 2011, O'Neill *et al* presented a three-state thermodynamic analysis of cell survival data in HepG2 cells (*i.e.* liver carcinoma).[91] The governing reaction formulation was actually identical to Equation 5, except the simplifying assumptions that reduce the relation to a single-step irreversible reaction were relaxed:

$$A \underset{k_b}{\overset{k_f}{\rightleftarrows}} V \xrightarrow{k_f} D \tag{34}$$

where: A and D are the live and dead cell populations, respectively, and V are "vulnerable" cells, a postulated state between live and dead that mirrors the activated state, C* in Equation 5 — precisely why the authors passed up the golden opportunity to label them "zombie" cells I will never know. Of course, the sum of the 3 states must always be 1, so "V" can be eliminated by continuity constraints. The two dynamic state-space equations that result are:

$$\frac{dA}{dt} = -k_f A + k_b (1 - A - D) \tag{35a}$$

$$\frac{dD}{dt} = k_f (1 - A - D) \tag{35b}$$

In order to fit the data, the authors introduced a nonlinear form for the forward reaction velocity:

$$k_f = k_{f0}\, e^{\frac{T}{T_k}} (1 - A) \tag{36}$$

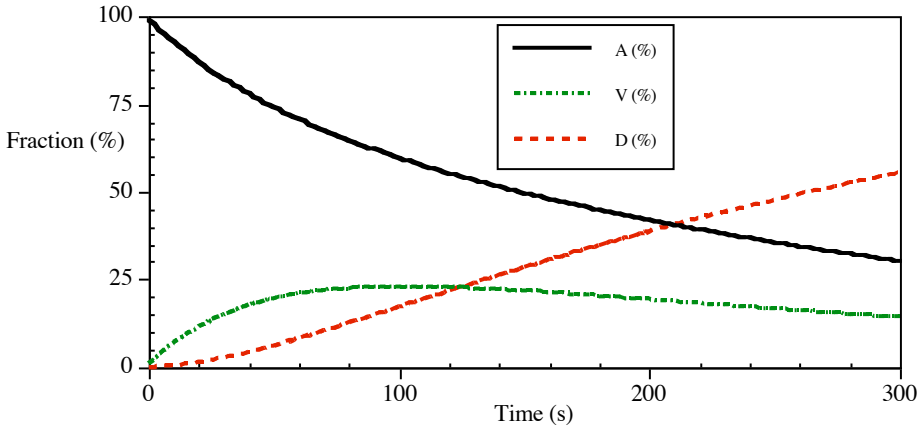

Fig. 18 (a)

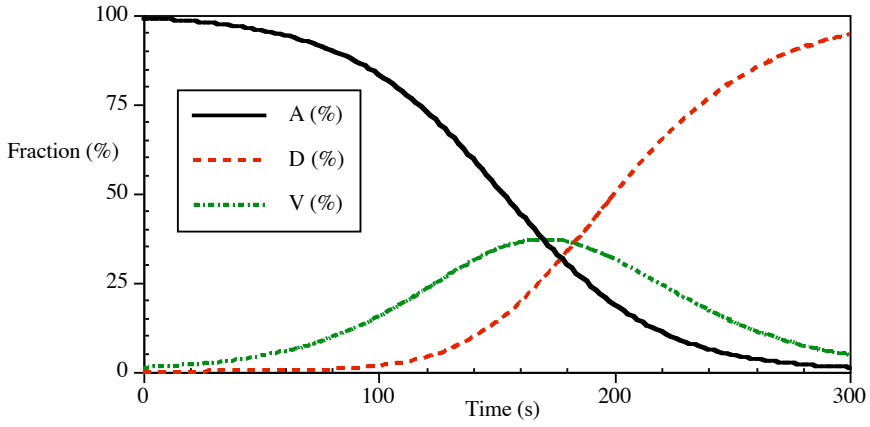

Fig. 18 (b)

Figure 18 Cell population predictions for two mathematical models. a) A single reversible reaction with constant reaction velocities: k_a = 0.007, k_b = 0.008 and k_c = 0.01 (s^{-1}). b) The O'Neill *et al.* model calculated at T = 90 C.[30]

To fit the HepG2 cell data, k_{f0} = 0.80x10^{-3} (s^{-1}), k_b = 0.25x10^{-3} (s^{-1}) and T_k = 24.6 (°C). When the nonlinear form for k_f is substituted into Equations 35, the result is very similar to a reduced form of the state-space relations from Eissing *et al*:

$$\frac{dA}{dt} = -k_{fp}[A] + k_{fp}[A][A] + k_b(1 - A - D) \tag{37a}$$

$$\frac{dD}{dt} = k_{fp}(1 - A - D) - k_{fp}[A] + k_{fp}[A][A] + k_{fp}[A][D] \qquad (37b)$$

Here k_{fp} includes the temperature dependence in k_f (*i.e.* everything except the 1-A term). The three postulated association reaction forms are the likely origin of the delay features in the model. That is, relaxing the irreversibility assumption alone does not generate much of a delay feature. To see why this is so, we can look at a reversible reaction with constant reaction velocities, as in Figure 18a. The plot has some of the features of the calculation from the O'Neill model, but no where near the delay in the D(t) population of Fig. 18b.

There is another important lesson embedded in these two models. The reversible reaction has a decay in the A population that is accurately fit by a single exponential. The rise in the D population is not fit by an exponential function owing to the effect of the V population dynamic. Consequently, if the particular assay used to identify thermal damage follows the A population, and the process is governed by a simple reversible reaction with constant velocities, then an Arrhenius model should fit rather precisely. Under the same conditions, an assay following the D population will not conform to Arrhenius analysis. In any event, the presence of an identifiable delay in the development of the shoulder region in these curves establishes that a classical Arrhenius approach will not be adequate. This observation may at least partially explain why Arrhenius models fit some cell survival data quite well, such as the SN12 human renal carcinoma cell data,[67] but fail miserably in other measurements.

2. Adding a Delay to the Arrhenius Model

The primary feature missing from an Arrhenius calculation is the delay in the shoulder region. This can be seen more clearly in a logarithmic plot, as in Figure 23. The CHO cell data from Figure 11 at a temperature of 43.5 C is compared to the classical Arrhenius prediction using the coefficients derived from the constant rate portion of the data ensemble.

In fact, we care little for an accurate calculation in the shoulder region since we wish to identify when the heating will be effective. The primary criticism of the Arrhenius approach is that it always over-predicts cell death leading to an unacceptably optimistic assessment. What if we just added a delay to the Arrhenius calculation? That will discard data in the shoulder region, but could give much improved and more realistic results overall in the constant rate region beyond the shoulder where most of the cell death actually occurs.

Looking at the same 43.5 C curve, the constant rate region (solid squares in Figure 24) is fit by:

$$C(t) = 111.2\, e^{[-0.14323\, t]} \qquad r^2 = 0.9995 \qquad (38)$$

where t is in minutes. The resulting reaction velocity in the constant rate region, k = 2.372×10^{-3} (s^{-1}) — compare this value to k = 2.092×10^{-3} (s^{-1}) from the direct calculation based

on the Arrhenius coefficients used to plot Fig. 19. The calculated time delay from the fit curve is $\Delta t_d = \ln\{111.2\}/(2.372 \times 10^{-3}) = 1986$ (s), or 33.1 (min).

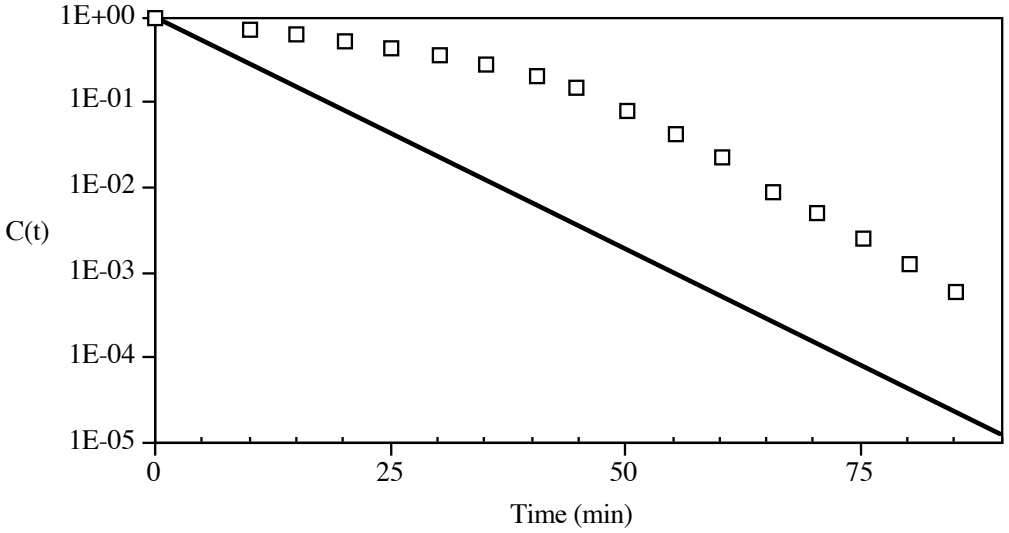

Figure 19 Arrhenius prediction of the surviving fraction of CHO cells at 43.5 C (line) compared with reported data (open squares). Arrhenius model coefficients were: $A = 9.386 \times 10^{101}$ and $E_a = 6.344 \times 10^5$ (J mol^{-1}).

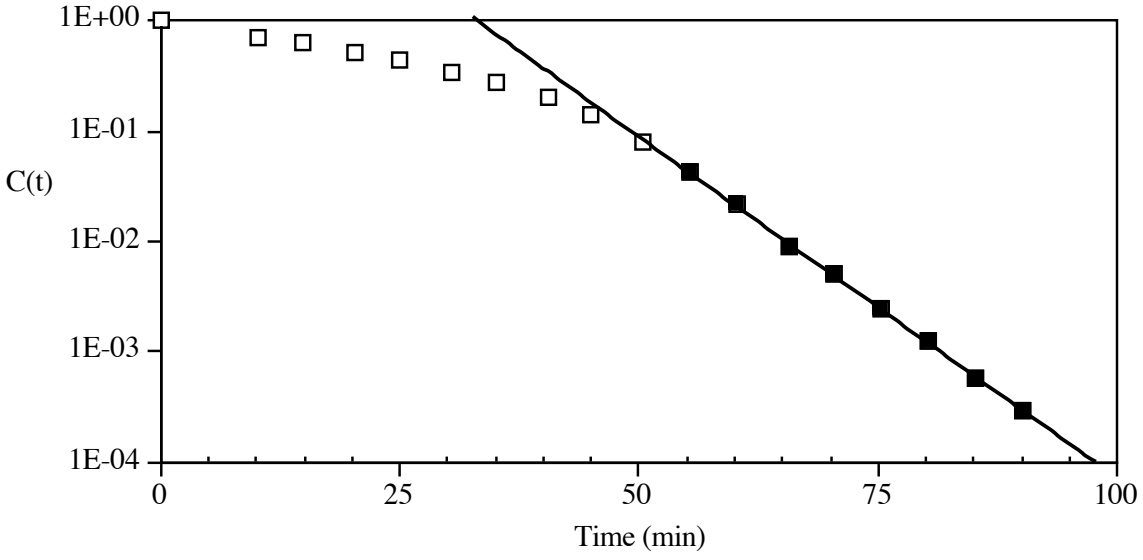

Figure 20 Exponential fit to constant rate region (solid squares) for CHO cells at 43.5 C.[92]

Similar fits applied to the other CHO curves from Figure 12 gives a linear fit for the required time delay:

$$\Delta t_d\,(s) = 26062 - 555.8\,T\,(C) \qquad T_{max} = 46.9\ C \tag{39}$$

and the maximum temperature for which Δt_d is positive is 46.9 C.

In Figure 21 the resulting fit to CHO data using Arrhenius coefficients derived from the constant rate regions and the time delay from Equation (39) gives better predictions of the measured cell death than without the time delay term. A much better overall improvement in the prediction was obtained from the PC-3 cell data using the same method.[93] PC-3 cells are a human prostate cancer cell line. Several of the time delay fit curves to PC-3 data are plotted in Figure 22.

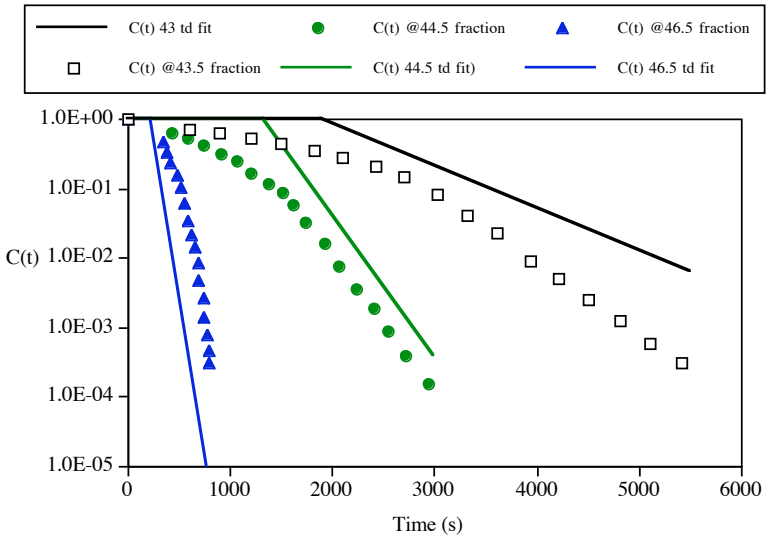

Figure 21 Modified Arrhenius fit to representative CHO cell data including time delay.[92]

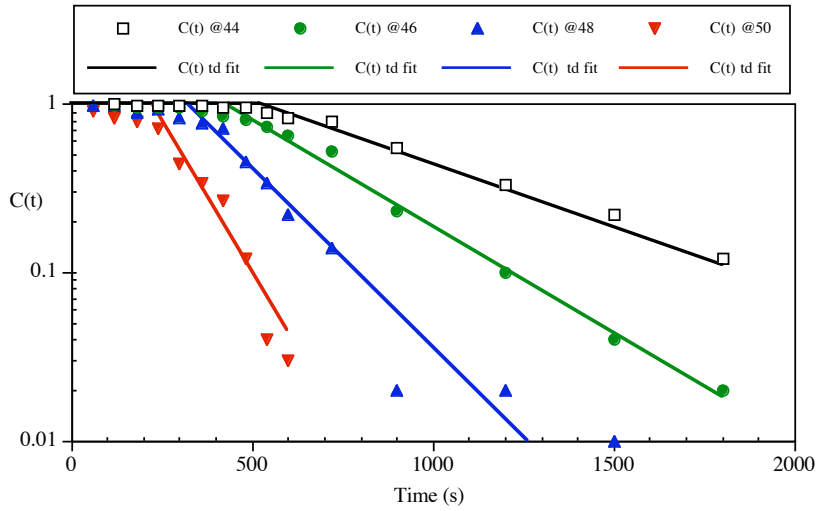

Figure 22 Modified Arrhenius fit to PC-3 cell data including time delay.[92]

Table 5 Modified Arrhenius fit relations including time delay. The time delay is expressed in seconds and curve fit coefficients a = offset (s) and b = slope (s/C).[92]

Cell Line	Offset, a (s)	Slope, b (s/C)	T_{max} (C)	A (s^{-1})	E_a (J/mole)
CHO	26,062	555.8	46.9	7.25×10^{100}	6.28×10^{5}
PC-3	2,703	49.6	54.5	6.75×10^{31}	2.22×10^{5}

E. Summary of Thermal Damage Predictions and Cell Death Processes.

First order kinetic models for tissue damage based on a single-step irreversible reaction are useful for predicting trends in thermal damage experiments. The classical Arrhenius model approach works very well for structural proteins and at higher temperatures where intrinsic cell processes have been overwhelmed — critical temperatures for known processes range from about 50 to 90 C plus. These models can be used to make direct comparisons between numerical predictions of damage and histologic results; something that cannot, as yet, be achieved any other way. A very careful definition of the particular histologic end point is necessary. Also, to avoid the arbitrariness that characterizes many of the early damage studies, it is essential that a quantitatively measurable damage measure be identified. Birefringence intensity is one such variable. Other excellent candidates include, for example, vital stain uptakes, fluorescence, and changes in electrical or optical properties.

The single reaction kinetics models do not predict the early phases of cell survival experiments. The probable proteinaceous mechanisms at work consist of complex multi-reaction sequences in functional proteins (*i.e.* enzymes) with multiple feedback regulatory pathways that the single reaction description cannot hope to duplicate. Several reports that employ enzyme substrate kinetic approaches perform better in those instances. All of the successful models of thermal damage and cell death include at least one constant-rate Arrhenius-like term.

In part because of the effects of biologic inhomogeneities and random fluctuations in tissue characteristics, and in part due to the difficulty of resolving small temperature differences, thermal damage data are inherently noisy. Certainly, even though the results of a particular experiment may eventually prove impossible to duplicate in numerical models, a rather careful analysis of the trends which one would obtain from, say, changing applied power, heating geometry and duration can be studied in detail in the numerical model and on a spatial scale similar to that of microscopic observation. Also, a numerical model allows dissection of the transient development of thermal damage — something that cannot be achieved in any other way. So, while there are many uncertainties associated with kinetic models of thermal damage, they can be extremely illuminating and helpful in dosimetry planning.

V. Implementing Thermal Damage Models in COMSOL

Some of these suggestions were written for Comsol 3.5a. The names and locations of some of the functions and other categories changed in versions 4.3 and later. All of them are there somewhere, plus many additional features. Sorry, I did not have time to go through and update everything.

1. Hyperthermia: CEM 43 Damage Models

Starting with a functional FEM model that already calculates transient temperature fields (usually a Bioheat Equation Mode), under the "Multiphysics" main menu heading "Model Navigator" choose an appropriate mode to add. All that is needed is to integrate some function of the temperature field over time. The "PDE, coefficient form" model mode is ideal for damage calculations, but any transient mode can be used for the integration. For a 2D axisymmetric geometry the selections are somewhat limited — I suggest using a simple "transient heat equation" mode (conduction only is just fine). Before adding the mode, it will be helpful to change the Application Mode Name to something more meaningful, like "Hyperthermia" or "HyperT", and the Dependent Variable to something like "CEM43". This will make it easier to keep track of added mode significance and identity. Be sure the mode "Properties" are set to "Transient", then add the mode. Close the Model Navigator window.

Be sure that the main model geometry window is set to the newly added "CEM43" mode. Under the main menu heading "Physics", select "Subdomain Settings". Select all subdomains for which you want the CEM 43 calculations to be performed and click "Active in This Domain". In the "PDE coefficient" mode there is a fairly long list of subdomain coefficients, some of which (the Greek characters, α, β, and γ) are vectors. The goal is to accomplish a time integration so set δ_a (time scaling) to "1" and f (the forcing function) to "min(dRate_low, dRate_high)". In a "heat equation" mode make $d = \rho = c = 1$ and $k = 0$ (no spatial gradients), and make the volumetric source term Q = min(dRate_low, dRate_high). The two rates correspond to temperatures above and below the breakpoint, and the minimum value is always the one wanted. Be sure that all other coefficients are zero. Check to see that the initial value is also <u>zero</u> (IMPORTANT since the default might be 310.15 K, depending on the mode).

Under the main menu heading "Global Definitions", select "Parameters". Define "Tbreak", "Rupper" and "Rlower" to be as desired (or other appropriate constant names). Then, under the same menu heading, select "Variables" and create the two expressions needed for the forcing function, "dRate_low" and "dRate_high". You will need Tbreak, Rupper and Rlower values for each tissue type. For the respective expressions enter:

(Rlower^(Tbreak-T_ht))/60 (Rupper^(Tbreak-T_ht))/60 (23)

Here "T_ht" is the calculated transient temperature field from the heat equation model, so use whatever variable name is used in that mode. Be careful about Celsius or Kelvin degrees here. Tbreak has to match T_ht units. You have to divide by 60 because the time axis is in seconds and the rate calculation is "per minute".

It remains to set the boundary conditions. Under the main menu heading "Physics", select "Boundary Settings". Select all external boundaries and make them "Neumann Boundary Condition" with zero flux.

Solve the problem using the same settings as for the transient temperature calculations. With the new added mode(s) it will take slightly longer to solve.

2. Arrhenius Kinetics Models

Damage processes can be modeled as first-order rate processes for which two experimentally derived coefficients are sufficient, commonly referred to as an Arrhenius damage model. Thermal damage in this formulation is exponentially/hyperbolically dependent on temperature and linearly dependent on time of exposure. The rate process models apply well to the prediction of damage thresholds, and less well as the damage becomes complete since several of the fundamental assumptions are violated. By recasting the damage model(s) in terms of C(t), one can include many thermodynamically-independent damage processes at work in parallel. Simply apply a separate set of coefficients and a model mode for each process under study.

Follow the same strategy to add an appropriate mode as for the CEM43 calculation, as described above. I suggest giving this mode the name "Arrhenius" and making the Dependent Variable "W", since W is the character for Ω in "Symbol" font, which is not available in Comsol. For several damage modes in parallel you can use something specific, like "Wpc3", or "Wat1" ... Note that you can superpose the hyperthermia and Arrhenius damage models in the same calculation this way. Also, remember to be sure that the added mode is transient.

The calculation based on Ω is a little more sensitive since it can become very large with small changes in temperature. It is best to move the frequency factor, A, into the exponential, and to be absolutely sure that a negative value is never obtained (although that is very unlikely). Define parameters "ln_A" = ln{A}, "Ea" = the activation energy, and "Rgas" = 8.3143, the gas constant. We need (dW/dt) as the forcing function for the mode (either "f" or "Q" ... i.e. an added "Heat Source"). I suggest using two steps, first under "Variables":

$$\mathrm{dW\_est} = max\left(0, exp\left(\mathrm{ln\_A} - \mathrm{Ea} / \left(\mathrm{Rgas} * \mathrm{T\_ht}\right)\right)\right). \tag{24}$$

where: "T_ht" is the temperature from the thermal model (K) — it might be called "mod1.T" or something similar.

Then, to control the magnitude of dΩ/dt so that the resulting exponentials are well behaved define the integrating expression:

$$\mathrm{dWdt} = min\left(10, \mathrm{dW\_est}\right). \tag{25}$$

This will prevent exponentiating unruly numbers when calculating the damage field. In the "Post Processing" mode you can plot the damage probability (%):

$$\text{Damage}(\%) = 100 * \left(1 - exp\left(-\text{W}\right)\right) \tag{26}$$

You can superpose as many of these thermal damage models as you want by adding a multiphysics mode for each process, each with its own set of ln{A} and E_a values.

3. Including a Time Delay in a Arrhenius Model

The required time delay can either be implemented as a direct calculation from the calculated linear fit (t_d = a - bT), in which some error may arise from not accumulating the transient time affects on the exposure, or by adding an additional integrating mode.

In the first approach the local temperature establishes the required delay. Then for all time in which $t > t_d$ turn the damage accumulation process on using a conditional:

$$\text{dWdt} = \left(\text{t} >= \text{td}\right) * \text{dWdt} = min\left(10, \text{dW\_est}\right) \tag{27}$$

You may want to add some controls to be sure that td doesn't go negative, although this shouldn't strictly be necessary.

Calculating directly from the time delay linear fit accumulates no error if dT/dt is a constant, and only 10 to 30 s if it follows a square root of time history up to about 60 C. The accumulating effects of T(t) on td can be included by adding one more integrating mode, integrating:

$$\text{td\_eff} = \text{a} - \int \text{b}\left(\frac{\partial \text{T}}{\partial \text{t}}\right) \text{dt} \tag{28}$$

and (∂T/∂t) is available from a heat transfer mode as "Tt", or similar variable name.

References

[1] J.H. Wilmore and D.L. Costill, *The Physiology of Sport and Exercise*, Champaign, IL: Human Kinetics, 1994.

[2] L. Delavallee, L. Cabon, P. Galan-Malo, K.L. Hans, and A.S. Santos, "AIF-mediated caspase-independent necroptosis: a new chance for targeted therapeutics," *IUBMB life*, vol. 63, (no. 4), pp. 221-232, 2011.

[3] C.C.T. Smith and Y. D.M., "Necroptosis, necrostatins and tissue injury," *Journal of Cellular and Molecular Medicine*, vol. 15, (no. 9), pp. 1797-1806, 2011.

[4] T. Vanden Berghe, N. Vanlangenakker, E. Parthoens, W. Deckers, M. Devos, N. Festjens, C.J. Guerin, U.T. Brunk, W. Declercq, and P. Vandenabeele, "Necroptosis, necrosis and secondary necrosis converge on similar cellular disintegration features," *Cell Death and Differentiation*, vol. 17, (no. 6), pp. 922-930, 2010.

[5] P. Vandenabeele, L. Galluzzi, T. Vanden Berghe, and G. Kroemer, "Molecular mechanisms of necroptosis: an ordered cellular explosion. ," *Nature Reviews. Molecular Cell Biology*, vol. 11, (no. 10), pp. 700-714, 2010.
[6] A.L. Edinger and C.B. Thompson, "Defective autophagy leads to cancer," *Cancer Cell*, vol. 4, (no. 6), pp. 422-424, 2003.
[7] T.M. Cox and M.B. Cachon-Gonzalez, "The cellular pathology of lysosomal diseases," *The Journal of Pathology*, vol. 226, (no. 2), pp. 241-254, 2012.
[8] F. Chen, C.-C. Wang, E. Kim, and L.E. Harrison, "Hyperthermia in combination with oxidative stress induces autophagic cell death in HT-29 colon cancer cells," *Cell Biology International*, vol. 32, (no. 7), pp. 715-723, 2008.
[9] G. Xiao, "Autophagy and NF-kappaB: fight for fate," *Cytokine & Growth Factor Reviews*, vol. 18, (no. 3-4), pp. 233-243, 2007.
[10] Y. Zhang and S.K. Calderwood, "Autophagy, protein aggregation and hyperthermia: a mini-review," *International Journal of Hyperthermia*, vol. 27, (no. 5), pp. 409-414, 2011.
[11] T. Bergsbaken, S.L. Fink, A.B. den Hartigh, W.P. Loomis, and B.T. Cookson, "Coordinated host responses during pyroptosis: caspase-1-dependent lysosome exocytosis and inflammatory cytokine maturation.," *Journal of Immunology*, vol. 187, (no. 5), pp. 2748-2754, 2011.
[12] F.C. Henriques and A.R. Moritz, "Studies of thermal injury in the conduction of heat to and through skin and the temperatures attained therein: A theoretical and experimental investigation," *American Journal of Pathology*, vol. 23, pp. 531-549, 1947.
[13] F.C. Henriques, "Studies of Thermal Injury, V. The predictability and significance of thermally induced rate processes leading to irreversible epidermal injury," *Archives of Pathology*, vol. 43, pp. 489-502, 1947.
[14] A.R. Moritz, "Studies of thermal injury III. The pathology and pathogenesis of cutaneous burns: An experimental study," *American Journal of Pathology*, vol. 23, pp. 915-934, 1947.
[15] A.R. Moritz and F.C. Henriques, "Studies in thermal injury II: the relative importance of time and surface temperature in the causation of cutaneous burns," *American Journal of Pathology*, vol. 23, pp. 695-720, 1947.
[16] S. Arrhenius, "Uber die Reaktionsgeschwindigkeit bei der Inversion von Rohrzucker durch Sauren (On the Reaction Rate in the Inversion of Cane Sugar by Acids)," *Z. Phys. Chem.*, vol. 4, pp. 226-248, 1889.
[17] F.H. Johnson, H. Eyring, and B.J. Stover, *The Theory of Rate Processes In Biology and Medicine*, New York: John Wiley & Sons, 1974.
[18] S. Arrhenius, *Quantitative Laws in Biological Chemistry*, London: G. Bell & Sons, 1915.
[19] H. Eyring, "The Energy of Activation for Bimolecular Reactions Involving Hydrogen and the Halogens, According to Quantum Mechanics," *Journal of the American Chemical Society*, vol. 53, pp. 2537-2549, 1931.
[20] H. Eyring, "The Activated Complex in Chemical Reactions," *Journal of Chemical Physics*, vol. 3, (no. 2), pp. 107-115, 1935.
[21] H. Eyring, H. Gershinowitz, and C.E. Sun, "The Absolute Rate of Homogeneous Atomic Reactions " *Journal of Chemical Physics*, vol. 3, (no. 12), pp. 786-796, 1935.
[22] S.H. Maron and J.B. Lando, *Fundamentals of Physical Chemistry*, New York: Macmillan Publishing Co., 1974.
[23] H. Eyring and M. Polyani, "Über Einfache Gasreaktionen (On Simple Gas Reactions)," *Zeitschrift fur Physikalische Chemie B*, vol. 12, pp. 279-311, 1931.
[24] H. Eyring and A.E. Stearn, "The Application of the Theory of Absolute Reaction Rates to Proteins," *Chemical Reviews*, vol. 24, pp. 253-270, 1939.
[25] B. Rosenberg, G. Kemeny, R.C. Switzer, and T.C. Hamilton, "Quantitative Evidence for Protein Denaturation as the Cause of Thermal Death," *Nature*, vol. 232, pp. 471-473, 1971.
[26] X. He and J.C. Bischof, "Quantification of Temperature and Injury Response in Thermal Therapy and Cryosurgery," *Critical Reviews in Biomedical Engineering*, vol. 31, (no. 5 & 6), pp. 355-421, 2003.

[27] N.T. Wright, "On a relationship between the Arrhenius parameters from thermal damage studies," *Journal of Biomechanical Engineering*, vol. 125, (no. 2), pp. 300-304, 2003.
[28] C.A. Miles and M. Ghelashvili, "Polymer-in-a-Box Mechanism for the Thermal Stabilization of Collagen Molecules in Fibers," *Biophysics Journal*, vol. 76, pp. 3243-3252, 1999.
[29] X. He, S. Bhowmick, and J.C. Bischof, "Thermal Therapy in Urologic Systems: A Comparison of Arrhenius and Thermal Isoeffective Dose Models in Predicting Hyperthermic Injury," *Journal of Biomechanical Engineering*, vol. 131, pp. 745071, 2009.
[30] J.A. Pearce, "Comparative analysis of mathematical models of cell death and thermal damage processes," *International Journal of Hyperthermia*, vol. 29, (no. 4), pp. 262-280, 2013.
[31] J.A. Pearce, S.L.M.D. Thomsen, H. Vijverberg, and T.J. McMurray, "Kinetics for birefringence changes in thermally coagulated rat skin collagen," in, 1993, pp. Pages.
[32] M.E. Nimmi, "Molecular Structures and Functions," in Collagen: Volume I Biochemistry, vol. I. Biochemistry, Boca Raton, FL: CRC Press, 1988.
[33] J.A. Pearce, "Models for Thermal Damage in Tissues: Processes and Applications," *Critical Reviews in Biomedical Engineering*, vol. 38, (no. 1), pp. 1-20, 2010.
[34] S.S. Chen, N.T. Wright, and J.D. Humphrey, "Heat-induced changes in the mechanics of a collagenous tissue: Isothermal free shrinkage," *Journal of Biomechanical Engineering*, vol. 119, (no. 4), pp. 372-378, 1997.
[35] S.S. Chen, N.T. Wright, and J.D. Humphrey, "Heat-induced changes in the mechanics of a collagenous tissue: isothermal, isotonic shrinkage," *Journal of Biomechanical Engineering*, vol. 120, pp. 382-388, 1998.
[36] S.S. Chen, N.T. Wright, and J.D. Humphrey, "Phenomenological evolution equations for heat-induced shrinkage of a collagenous tissue," *IEEE Transactions on Biomedical Engineering*, vol. 45, pp. 1234-1240, 1998.
[37] J.A. Pearce, "Relationship between Arrhenius models of thermal damage and the CEM 43 thermal dose," in Proc. Energy-based Treatment of Tissue and Assessment V, 2009, pp. Pages.
[38] A.J. Welch and G.D. Polhamus, "Measurement and prediction of thermal injury in the retina of Rhesus monkey," *IEEE Transactions on Biomedical Engineering*, vol. 31, pp. 633-644, 1984.
[39] A.N. Takata, "Development of criterion for skin burns," *Aerospace Medicine*, vol. 45, pp. 634-637, 1974.
[40] R. Birngruber, F. Hillenkamp, and V.P. Gabel, "Theoretical investigations of laser thermal retinal injury," *Health Physics*, vol. 48, (no. 6), pp. 781-796, 1985.
[41] S. Thomsen, J.A. Pearce, and W.F. Cheong, "Changes in birefringence as markers of thermal damage in tissues," *IEEE Trans Biomed Eng*, vol. 36, (no. 12), pp. 1174-9, Dec 1989.
[42] S.L. Jacques and M.O. Gaeeni, "Thermally induced changes in optical properties of heart," *IEEE Eng. Med. Biol. Mag.*, (no. 11), pp. 1199-1200, 1989.
[43] K.R. Diller and G.A. Klutke, "Accuracy analysis of the Henriques model for predicting thermal burn injury," in Proc. Advances in Bioheat and Mass Transfer, 1993, pp. Pages.
[44] J.A. Weaver and A.M. Stoll, "Mathematical model of skin exposed to thermal radiation," *Aerospace Medicine*, vol. 40, (no. 1), pp. 24-30, 1967.
[45] J.T. Beckham, G.J. Wilmink, M.A. Mackanos, K. Takahashi, C.H. Contag, T. Takahashi, and E.D. Jansen, "Role of HSP70 in Cellular Thermotolerance," *Lasers in Surgery and Medicine*, vol. 40, pp. 704-715, 2008.
[46] Y.C. Wu, "A Modified Criterion for predicting thermal injury," National Bureau of Standards, Washington, D.C.1982.
[47] C.H. Fugitt, "A Rate Process Theory of Thermal Injury," in Book A Rate Process Theory of Thermal Injury, *Series A Rate Process Theory of Thermal Injury*, Editor ed.^eds., City: Armed Forces Special Weapons Project, 1955.
[48] A.N. Takata and e. al., "Thermal model of laser induced eye damage," Brooks AFB TX, Chicago, IL1974.
[49] A. Vassiliadis, H.C. Christian, and K.G. Dedrick, "Ocular laser threshold investigations," Brooks AFB TX1971.

[50] R. Birngruber, "Thermal modeling in biological tissue," in Lasers in Biology and Medicine: Plenum Publishing Corporation, 1980, pp. 77-97.
[51] C.A. Miles, "Kinetics of collagen denaturation in mammalian lens capsules studied by diff erential scanning calorimetry," *International J. of Biology and Macrobiology*, vol. 15, pp. 265-271, 1993.
[52] S.L. Jacques and S.A. Prahl, "Modeling optical and thermal distributions in tissue during laser irradiation," *Lasers in Surgery & Medicine*, vol. 6, pp. 494-503, 1987.
[53] D.J. Maitland and J.T. Walsh, Jr., "Quantitative measurements of linear birefringence during heating of native collagen," *Lasers in Surgery and Medicine*, vol. 20, pp. 310-318, 1997.
[54] D.C. Gaylor, "Physical mechanism of cellular injury in electrical trauma," 1989.
[55] N.A. Moussa, E.N. Tell, and E.G. Cravalho, "Time progression of hemolysis of erythrocyte populations exposed to supraphysiological temperatures," *Journal of Biomechanical Engineering*, vol. 101, (no. 3), pp. 213-217, 1979.
[56] J.R. Lepock, H.E. Frey, H. Bayne, and J. Markus, "Relationship of Hyperthermia-induced Hemolysis of Human Erythrocytes to the Thermal Denaturation of Membrane Proteins," *Biochimica et Biophysica Acta*, vol. 980, pp. 191-201, 1989.
[57] S.T. Flock, L. Smith, and M.D. Waner, "Quantifying the effects on blood of irradiation with four different vascular-lesion lasers," in Proc. Laser-Tissue Interaction IV, 1993, pp. Pages.
[58] Y. Yang, A.J. Welch, and H.G. Rylander, "Rate process parameters of albumin," *Lasers in Surgery and Medicine*, vol. 11, pp. 188-190, 1991.
[59] S.L. Jacques, C. Newman, and X.Y. He, "Thermal coagulation of tissues: Liver studies indicate a distribution of rate parameters not a single rate parameter describes the coagulation process," in Proc. Proc. Winter Annual Meeting, 1991, pp. Pages.
[60] K. Matthewson, P. Coleridge-Smith, J.P. O'Sullivan, T.C. Northfield, and S.G. Brown, "Biological effects of intrahepatic neodymium:yttrium-aluminum-garnet laser photocoagulation in rats," *Gastroenterology*, vol. 93, pp. 550-557, 1987.
[61] D. Germain, P. Chevallier, A. Laurent, M. Savart, M. Wassef, and H. Saint-Jalmes, "MR monitoring of laser-induced lesions of the liver in vivo in a low-field open magnet: temperature mapping and lesion size prediction," *Journal of Magnetic Resonnace Imaging*, vol. 13, (no. 1), pp. 42-49, 2001.
[62] G. Reddy, M. Dreher, C. Rossman, B.J. Wood, and D. Haemmerich, "Cytotoxicity of hepatocellular carcinoma cells to hyperthermic and ablative temperatrue exposures: In vitro studies and mathematical modeling," *International Journal of Hyperthermia*, vol. 29, (no. 4), pp. 318-323, 2013.
[63] M.G. Skinner, S. Everts, A.D. Reid, I.A. Vitkin, L. Lilge, and M.D. Sherar, "Changes in optical properties of ex vivo rat prostate due to heating," *Physics in Medicine and Biology*, vol. 45, pp. 1375-1386, 2000.
[64] S. Bhowmick, D.J. Swanlund, and J.C. Bischof, "Supraphysiological Thermal Injury in Dunning AT-1 Prostate Tumor Cells," *Journal of Biomechanical Engineering*, vol. 122, (no. 1), pp. 51-59, 2000.
[65] X. He, S. McGee, J.E. Coad, F. Schmidlin, P.A. Iaizzo, D.J. Swanlund, S. Kluge, E. Rudie, and J.C. Bischof, "Investigation of the thermal and tissue injury behaviour in microwave thermal therapy using a porcine kidney model," *International Journal Of Hyperthermia*, vol. 20, (no. 6), pp. 567-593, 2004.
[66] M. Pop, A. Molckovsky, L. Chin, M.C. Kolios, M.A. Jewett, and M.D. Sherar, "Changes in dielectric properties at 460 kHz of kidney and fat during heating: importance for radio-frequency thermal therapy," *Phys Med Biol*, vol. 48, (no. 15), pp. 2509-25, Aug 7 2003.
[67] X. He and J.C. Bischof, "The Kinetics of Thermal Injury in Human Renal Carcinoma Cells," *Annals of Biomedical Engineering*, vol. 33, (no. 4), pp. 502-510, 2005.
[68] E.G. Cravalho, "Response of Cells to Supraphysiological Temperatures: Experimental Measurements and Kinetic Models," in Electrical Trauma. The pathology, manifestations and clinical management., R. C. Lee, E. G. Cravalho and J. F. Burke eds.: Cambridge Press, 1992.

[69] D.M. Green and K.R. Diller, "Measurement of Burn-induced Leakage of Macromolecules in Living Tissue," *Journal of Biomechanical Engineering*, vol. 100, (no. 3), pp. 153-158, 1978.
[70] S.J. Aggarwal, S.J. Shah, K.R. Diller, and C.R. Baxter, "Fluorescence Digital Microscopy of Interstitial Macromolecular Diffusion in Burn Injury," *Computers in Biology and Medicine*, vol. 19, (no. 4), pp. 245-261, 1989.
[71] J.L. Van Delft, J.A. Oosterhuis, E.R. Barthen, and A.M. Eijkelenboom, "Janus green vital staining of the cornea," *Documenta Ophthalmologica*, vol. 55, (no. 1-2), pp. 47-50, 1983.
[72] R.B. Bhisitkul, "Second generation vital stains in retinal surgery," *British Journal of Opthalmic Surgery*, vol. 87, (no. 6), pp. 664-665, 2003.
[73] D. Acosta and D.G. Wendel, "A permeability test for the study of mitochondrial injury inin vitro cultured heart muscle and endothelioid cells," *The Histochemical Journal*, vol. 7, (no. 1), pp. 45-56, 1975.
[74] S. Feldman, S. Glagov, R.W. Wissler, and R.H. Hughes, "Postmortem delineation of infarcted myocardium. Coronary perfusion with nitro blue tetrazolium.," *Archives Of Pathology & Laboratory Medicine*, vol. 100, (no. 1), pp. 55-58, 1976.
[75] B.R. Lucchesi, W.E. Burmeister, T.E. Lomas, and G.D. Abrams, "Ischemic changes in the canine heart as affected by the dimethyl quaternary analog of propranolol, UM-272 (SC-27761)," *The Journal Of Pharmacology And Experimental Therapeutics*, vol. 199, (no. 2), pp. 310-328, 1976.
[76] S.A. Sapareto, "Ch 1: The Biology of Hyperthermia In Vitro," in Physical Aspects of Hyperthermia, vol. Medical Physics Monograph No. 8, G. H. Nussbaum ed., New York, NY: Am. Inst. Phys., 1982.
[77] S.A. Sapareto, L.E. Hopwood, and W.C. Dewey, "Combined Effects of X Irradiation and Hyperthermia on CHO Cells for Various Temperatures and Orders of Application," *Radiation Research*, vol. 73, (no. 2), pp. 221-233, 1978.
[78] S.A. Sapareto, L.E. Hopwood, W.C. Dewey, M.R. Raju, and J.W. Gray, "Effects of hyperthermia on survival and progression of Chinese hamster ovary cells," *Cancer Research*, vol. 38, (no. 2), pp. 393-400, 1978.
[79] P. Bhowmick, J.E. Coad, S. Bhowmick, J.L. Pryor, T. Larson, d.l.R. J., and J.C. Bischof, "In vitro assessment of the efficacy of thermal therapy in human benign prostatic hyperplasia," *International J. of Hyperthermia*, vol. 20, (no. 4), pp. 412-439, 2004.
[80] K. McMillan, "1125-nm quantum dot laser for tonsil thermal therapy," in Proc. Thermal Treatment of Tissue: Energy Delivery and Assessment VI, 2011, pp. Pages.
[81] S. Bhowmick, D.J. Swanlund, and J.C. Bischof, "In vitro thermal therapy of AT-1 Dunning prostate tumours," *International Journal of Hyperthermia*, vol. 20, (no. 1), pp. 73–92, 2004.
[82] M.J. Borrelli, L.L. Thompson, C.A. Cain, and W.C. Dewey, "Time-temperature analysis of cell killing of BhK cells heated at temperatures in the range of 43.5 °C to 57.0 °C," *International Journal of Radiation Oncology and Biological Physics*, vol. 19, pp. 389 - 399, 1990.
[83] M. Przybylska, M. Bryszewska, and J. KedzioraKedziora, "Thermosensitivity of red blood cells from Down's syndrome individuals," *Bioelectrochemistry*, vol. 52, (no. 2), pp. 239-249, 2000.
[84] K.R. Diller, J.W. Valvano, and J.A. Pearce, "Bioheat Transfer," in CRC Handbook of Thermal Engineering, F. Kreith ed., Boca Raton: CRC Press, 2000, pp. 114-215.
[85] P. Vandenabeele, L. Galluzzi, T. Vanden Berghe, and G. Kroemer, "Molecular mechanisms of necroptosis: an ordered cellular explosion.," *Nature Reviews. Molecular Cell Biology*, vol. 11, (no. 10), pp. 700-714, 2010.
[86] P. Bernardi, L. Scorrano, R. Colonna, V. Petronilli, and F. Di Lisa, "Mitochondria and cell death. Mechanistic aspects and methodological issues," *European Journal Of Biochemistry*, vol. 264, (no. 3), pp. 687-701, 1999.
[87] Q. Remijsen, T. Vanden Berghe, E. Wirawan, B. Asselbergh, E. Parthoens, R. De Rycke, S. Noppen, M. Delforge, J. Willems, and P. Vandenabeele, "Neutrophil extracellular trap cell death requires both autophagy and superoxide generation," *Cell Research* vol. 21, (no. 2), pp. 290-304, 2011.

[88] T. Eissing, H. Conzelmann, E.D. Gilles, F. Allgower, E. Bullinger, and P. Scheurich, "Bistability analyses of a caspase activation model for receptor-induced apoptosis. ," *Journal of Biological Chemistry*, vol. 279, (no. 35), pp. 36892-36897, 2004.

[89] M. Mackey and J.L. Roti Roti, "A Model of Heat-induced Clonogenic Cell Death," *Journal of Theoretical Biology*, vol. 156, pp. 133 - 146, 1992.

[90] J.L. Roti Roti, "Cellular responses to hyperthermia (40–46 C): Cell killing and molecular events," *International Journal of Hyperthermia*, vol. 24, (no. 1), pp. 3 - 15, 2008.

[91] D.P. O'Neill, T. Peng, P. Stiegler, U. Mayrhauser, S. Koestenbauer, K. Tscheliessnigg, and S.J. Payne, "A Three-State Mathematical Model of Hyperthermic Cell Death," *Annals of Biomedical Engineering*, vol. 39, (no. 1), pp. 570 - 579, 2011.

[92] J.A. Pearce, "Improving Accuracy in Arrhenius Models of Cell Death: Adding a Temperature-dependent Time Delay," *Journal of Biomechanical Engineering*, vol. (submitted for review), 2015.

[93] Y. Feng, J.T. Oden, and M.N. Rylander, "A two-state cell damage model under hyperthermic conditions: Theory and in vitro experiments," *Journal of Biomechanical Engineering*, vol. 130, (no. 4), pp. 041016, 2008.